KfK 2659
März 1978

Application of Ion Beams for Modification and Analysis of Superconducting Materials with bbc, NaCl and A15 Structure

O. Meyer, G. Linker, J. M. Lombaard, B. Seeber
Institut für Angewandte Kernphysik

Kernforschungszentrum Karlsruhe

Solid State Communications, Vol. 22, pp. 603–607. 1977. Pergamon Press. Printed in Great Britain

CHANNELLING EFFECT MEASUREMENTS OF ^{4}He-INDUCED DAMAGE IN V_3Si SINGLE CRYSTALS

O. Meyer

Kernforschungszentrum Karlsruhe, Institut für Angewandte Kernphysik, P.O.B. 3640, D-7500 Karlsruhe, Federal Republic of Germany

and

B. Seeber

Forschungslaboratorium für Festkörperchemie, Universität München, Germany

(*Received* 25 *November* 1976 *by P.H. Dederichs*)

Disorder produced by 0.3 MeV ^{4}He ions in V_3Si has been analysed by 2 MeV ^{4}He ion channelling measurements. In the region of low damage level (near the surface) a narrowing of about 10% in the $\psi_{1/2}$ values and an increase in χ_{min} has been observed along the V chains in V_3Si. The empirical formulas from Barrett based on Monte Carlo Computer calculations have been used for several model calculations. The best fit to the observed results was obtained by assuming an average displacement of 0.115 Å of all V atoms from the chain.

V_3Si IS ONE OF the well-known superconducting compound with A15 structure. In this structure the superconducting transition temperature T_c seems to be related to the linear chains of the transition metal atoms. Irradiation of V_3Si thin films with He ions [1] was found to lower T_c as well as the electrical resistance ratio r [$r = \rho(300\,K)/\rho(25\,K)$]. The correlation between T_c and r has been observed in as-grown and in radiation damaged V_3Si sputtered films [2]. This correlation between T_c and r is therefore thought to be due to common defect centers, which produce large contributions to the electron scattering. The nature of this defect is not yet known. In this work channelling effect [3] measurements on ^{4}He-irradiated V_3Si single crystals have been undertaken in order to study the structure of this defect and the possible influence on the chain integrity.

V_3Si single crystals have been cut perpendicular to the [100] direction and surface preparation was performed by lapping and polishing with diamond paste followed by an etching procedure. ^{4}He ions have been implanted at room temperature with fluences between 0.9×10^{16} and $1.2 \times 10^{17}\,cm^{-2}$ at an energy of 300 keV. Backscattering and channelling analysis measurements have been performed with 2 MeV ^{4}He ions with fluences which are small compared to the implanted fluences.

Backscattering spectra from virgin and from implanted V_3Si crystals are shown in Fig. 1 for random and [100] aligned beam incidence. It can be seen that the ^{4}He ion backscattered from V atoms near the surface are well separated in energy from those backscattered from Si atoms. The angular scan measurements in order to obtain the critical angle, $\psi_{1/2}$, and the normalized minimum yield, χ_{min}, could be performed for the V sublattice. ($\psi_{1/2}$ is the half-angular width at half height between the minimum yield and the yield for a non-channelling direction; χ_{min} is the minimum yield normalized to the random yield). The close-packed V chains are strong rows according to their ability to steer particles as particles will be channelled in respect to these chains while travelling randomly with respect to the other Si and V rows parallel to the strong rows. Therefore the channelling characteristics of the close-packed chains will not be influenced by the presence of the other atom rows.

The [100] aligned spectra for the crystal implanted with 4×10^{16} and 10^{17} He ions cm^{-2} in Fig. 1 may be compared to that of the virgin crystal and will reflect the damage distribution induced by the implanted ^{4}He ions. In the surface region (~ 4000 Å thick) only a small increase in the dechannelling yield is observed whereas at the end of the implanted He ion range a large number of displaced atoms are produced as indicated by a large peak due to ^{4}He ions scattered from displaced host atoms. Angular tilt measurements have been performed close to the surface where the number of displacements per atom is about three orders of magnitude smaller than near the end of the He ion range. The window settings for the scans at depths of 560 and 2020 Å are indicated by horizontal bars in Fig. 1. The depth scale has been calculated by assuming the same energy loss for the aligned and random spectra. Care has been taken to use the same angular scan directions in successive runs with the implanted He ions dose as a parameter. The surface peak area which is proportional to the

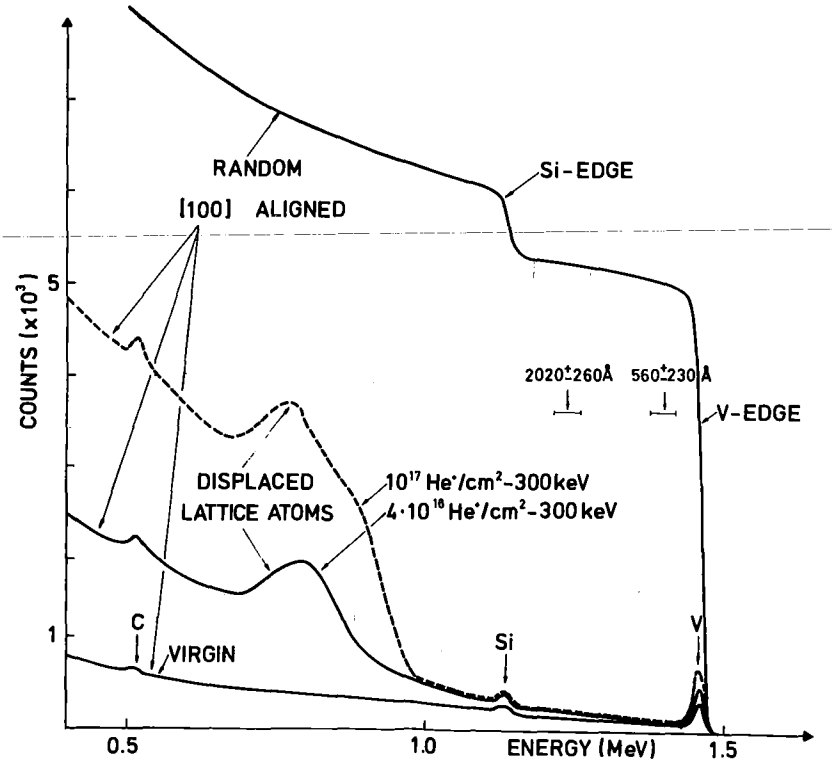

Fig. 1. Energy spectra of 2 MeV ^{4}He ions backscattered from a V_3Si single crystal. Included are the ⟨100⟩ aligned backscattering spectra after implantation of 4×10^{16} He^+cm^{-2} and 10^{17} He^+cm^{-2} at 300 keV.

number of V surface atoms and to displaced V atoms at the surface, due to the natural oxide, does not strongly affect χ_{min} as different surface peak areas have been observed for the same χ_{min} values of implanted samples (See Fig. 1). In Fig. 2 angular scans from a virgin crystal (x) are compared with the results obtained from the crystal after implantation of 4×10^{16} He cm^{-2} (•). In the implanted sample a considerable narrowing of the critical angle of the V atom chains and a slight increase of the minimum yield is observed. In Table 1 the measured values for $\psi_{1/2}$ and χ_{min} as a function of the fluence and depth are summarized. The narrowing of $\psi_{1/2}$ and an increase of χ_{min} starts for a fluence of 2×10^{16} and saturations occur for fluences above 4×10^{16} He cm^{-2}

As the T_c degradation in the implanted layer on the bulk V_3Si single crystal can not be measured, the values of T_c for V_3Si thin films as a function of He fluence, as measured by Poate *et al.* [1], have been taken and may be correlated with the observed decrease in $\psi_{1/2}$ and increase in χ_{min} with the fluence. As the energy E used in their experiment (2 MeV) is different from ours (0.3 MeV), the corresponding dose is scaled with E^{-1} [4]. Therefore it can be assumed that the same damage has been produced in both experiments and it can be seen from Table 2 that the decrease in T_c is accompanied by the decrease in $\psi_{1/2}$ and the increase in χ_{min}. The values of $\psi_{1/2}$ and χ_{min} presented in Table 2 are determined by extrapolation to zero target thickness (corresponding to zero energy loss). These extrapolated values may be compared to calculated values using the empirical formulas from Barret [5] based on Monte Carlo computer calculations:

$$\psi_{1/2} = 0.8 F_{RS}(1.2u_1/a)\psi_1 \qquad (1)$$

where

Table 1. Critical angle and minimum yield as a function of He *ion fluence at 300 keV*

Fluence (^{4}He cm^{-2})	Depth (Å)	$\psi_{1/2}$ (°)	χ_{min}
	560	0.72 ± 0.01	0.023
–	2020	0.63 ± 0.01	0.028
9.0×10^{15}	560	0.71	0.03
	2020	0.61	0.05
2.0×10^{16}	560	0.68	0.034
	2020	0.59	0.05
4.0×10^{16}	560	0.66	0.04
	2020	0.56	0.065
6.0×10^{16}	560	0.64	0.04
	2020	0.57	0.06
10^{17}	560	0.65	0.04
	2020	0.56	0.06
1.2×10^{17}	560	0.64	0.037
	2020	0.58	0.05

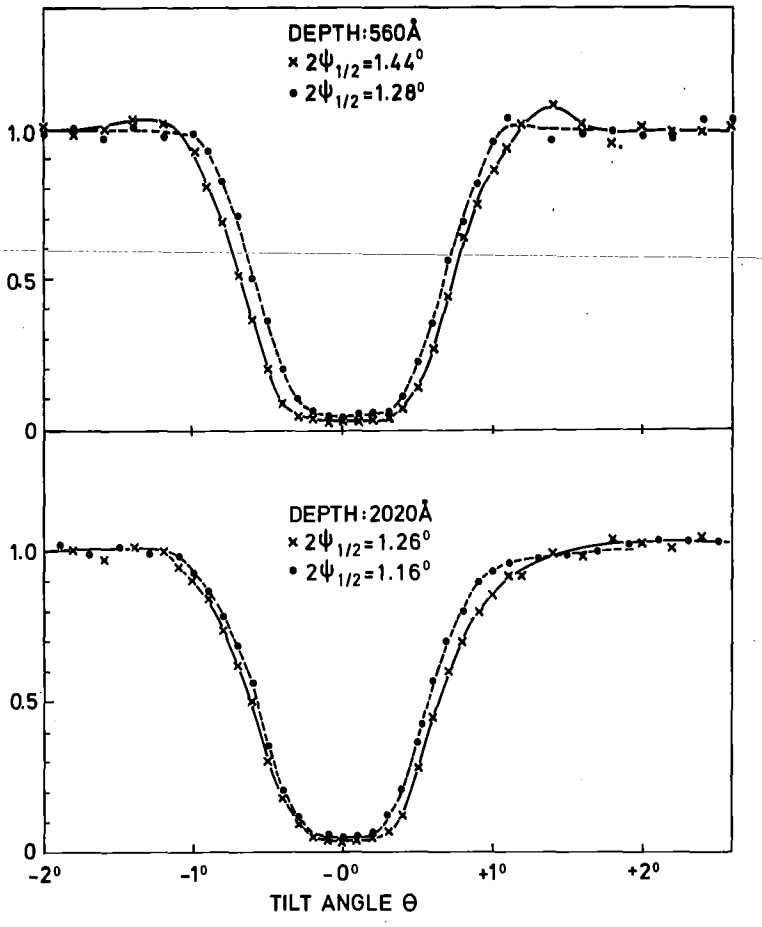

Fig. 2. Normalized angular yield profiles at different depth for the virgin crystal (x) and after implanting 4 x 10^{16} He^+cm^{-1} at 300 keV (•).

Table 2. Values of $\psi_{1/2}$ *and* χ_{min} *at zero target thickness of* He *fluenee (300 keV), lowering of* T_c *as a function of* He *fluence (2 MeV) as determined by Poate* et al. *[1]*

Fluence at 2 MeV [1]	Corresponding fluence at 300 keV	Average T_c (K) [1]	$\psi_{1/2}$	χ_{min}
	–	16.4	0.75 ± 0.01	0.020
6.0×10^{16}	9.0×10^{15}	12	0.75	0.022
1.3×10^{17}	2.0×10^{16}	7	0.72	0.028
2.6×10^{17}	4.0×10^{16}	3.5	0.70	0.03
4.0×10^{17}	6.0×10^{16}	2.5	0.67	0.032
6.6×10^{17}	10^{17}	2.5	0.68	0.04
8.0×10^{17}	1.2×10^{17}	–	0.67	0.032

$$\psi_1 = \left[\frac{2Z_1Z_2e^2}{d \cdot E}\right]^{1/2}$$

$$\chi_{min} = 18.8Ndu_1^2. \quad (2)$$

E is the energy of the analysing He ion beam, Z_1 and Z_2 are the atomic numbers of He and V, respectively, d is the distance between adjacent V atoms in the chain and a is the Thomas Fermi screening radius. u_1 is the root mean square (r.m.s.) thermal vibration amplitude perpendicular to the chain and N is the number of atoms per unit volume. F_{RS} is a tabulated function [5].

Using these formulas, agreement within 1% for $\psi_{1/2}$ of the virgin crystal can be obtained by choosing $\theta_D = 330$ K which corresponds to $u_1 = 0.088$ Å. This value for θ_D is in good agreement with the value of

300 K as measured for the V sublattice by neutron scattering [6]. The calculated contribution of the V atoms to χ_{min} ($\chi_{min} = 0.035$) is larger than the measured value at the surface ($\chi_{min} = 0.02$). The contribution of the close-packed V chains to χ_{min} is about 25%.

Several parameters in equations (1) and (2) have been varied in order to find the most probable explanation for the observed decrease in $\psi_{1/2}$ and increase in χ_{min} for the damaged crystals.

(i) Vacancies: Well separated vacancies are assumed to exist in the close-packed V chains, leading to an increase in the average d value. An unrealistically large concentration of vacancies (about 20%) are necessary in order to describe the observed decrease in $\psi_{1/2}$; this would decrease χ_{min} in contrast to the measured increase in χ_{min}.

(ii) Si atoms on V atom lattice sites: Antiside structure defects are assumed to exist where V atoms have been replaced by Si atoms and this influences the average value of Z_2 in the V chain. About 50% Si atoms on V sites are necessary to fit the observed values of $\psi_{1/2}$; χ_{min} is not affected. This number is large compared to the assumed 10 to 20% antiside structure defects which are thought to cause a T_c degradation below 3 K [7].

(iii) Displacements: The most probable explanation of the results is the assumption of small V atom displacements from the row. The case of an isotropic Gaussian distribution of displacements from the lattice sites can be simulated by increasing the r.m.s. vibrational amplitude. Assuming an average displacement of 0.115 Å for all V atoms from the row, values of 0.68° for $\psi_{1/2}$ and 0.04 for χ_{min} are obtained. This displacement value is slightly larger than the r.m.s thermal vibrational amplitude of 0.088 Å perpendicular to row. It is unrealistic however to assume an increase of the thermal vibrational amplitude by such an amount. In the calculation only an average displacement of all V atoms has been assumed which will represent a lower limit. Larger displacements of fewer V atoms will not be considered here as this assumption would cause an inflection point in the angular tilt curve [8] which is not observed.

The large backscattering peak at the end of the ^{4}He ion range cannot be explained by small displacements from the row. This peak stems from He ions, which have been backscattered from V atoms displaced into the channels. Indeed it has been observed, that 10^{14} Kr^+cm^{-2} (50 keV) implanted into V_3Si at RT render the crystal completely amorphous [9]. The He induced damage profile in V_3Si is very similar to profiles of deuteron damage found for Si and Ge where also small displacements from the row have been observed [10]. This similarity which is in contrast to what is usually observed in metals, in V for example [11] where most of the damage anneals at RT, indicates that covalent bondings as in the semiconductors, also prevails in V_3Si. Strong covalent bonding between adjacent V atoms in V_3Si has indeed been observed with X-ray diffraction [12].

Our calculations show that 10% antiside structure defects cannot explain the narrowing of the critical angle in contrast to assumptions made in order to explain the observed degradation in T_c for neutron induced damage in A15 structures [7]. However, small average displacement of all V atoms from the row will fit the critical angle of the damaged crystals and will drive χ_{min} in the right direction. So our results support the idea [2] that the common defect structure as discussed above consists of numerous small bond-bending distortions rather than of vacancies and/or antiside structure defects. Strain fields from a few bond breaking defects might cause the existence of the observed average displacement which we think is responsible for the degradation of T_c.

REFERENCES

1. POATE J.M., DYNES R.L., TESTARDI L.R. & HAMMOND R.H., 3. Rochester Conference on Superconductivity, April 30–May 1 (1976).
2. TESTARDI L.R., POATE J.M. & LEVINSTEIN H.J., *Phys. Rev. Lett.* **37**, 637 (1976).
3. For reviews on the channelling technique see for example: GEMMEL D.S.,*Rev. Mod. Phys.* **46**, No. 1 (1974); MORGAN D.V. (Ed.), *Channelling'*. Wiley, London (1973).
4. THOMPSON M.W., *Defects and Radiation Damage in Metals.* Cambridge University Press (1969).
5. BARRET J.H., *Phys. Rev.* **B3**, 1527 (1971).
6. SCHWEISS P., KFK 2054, p. 12 (1974).
7. SWEEDLER A.R., SCHWEITZER D.G. & WEBB G.W., *Phys. Rev. Lett.* **33**, 168 (1974).

8. PICRAUX S.T., BROWN W.L. & GIBSON W.M., *Phys. Rev.* **B6**, 1382 (1972).
9. GEERK J., LINKER G., MEYER O. & SEEBER B., KFK 2357, p. 110 (1976) and unpublished results.
10. BAERI P., CAMPISANO S.U., FOTI G., RIMINI E. & DAVIES J.A., *Appl. Phys. Lett.* **26**, 424 (1975).
11. GETTINGS M., MEYER O. & LINKER G., *Rad. Effects* **21**, 51 (1974).
12. STAUDENMANN J.L., COPPENS P. & MULLER J., *Solid State Commun.* **19**, 29 (1976).

Note added in proof: Recent measurements in the [110] direction show an increase of the average displacement from 0.061 to 0.1 Å after He ion bombardment, indicating that the displacement is not simply perpendicular to the row.

Radiation Effects
1978, Vol. 36, pp. 83–89

CHANNELING STUDIES IN CARBON IMPLANTED NbC-SINGLE CRYSTALS

J. M. LOMBAARD† and O. MEYER

Kernforschungszentrum Karlsruhe, Institut für Angewandte Kernphysik, D-7500 Karlsruhe, Postfach 3640, Federal Republic of Germany

(*Received August 18, 1977; in final form November 3, 1977*)

Critical angles and minimum yields have been measured for the Nb- and the C-rows in ⟨110⟩-aligned $NbC_{0.89}$ and have been compared to calculated values. Similar measurements have been performed in C-implanted NbC single crystals. Differences in the dechanneling yields of the Nb- and C-sublattice have been found indicating an additional damage component in the C-sublattice.

INTRODUCTION

The superconducting transition temperature T_c of NbC with B1 structure strongly depends on the composition.[1] The maximum T_c-value that can be obtained in the equilibrium phase $NbC_{0.98}$ produced by C-diffusion into $NbC_{0.89}$ single crystals was found to be 11.1 K.[2] By additional C-implantation T_c has been increased up to 11.6 K.[3] During C-implantation radiation damage has been produced and annealing was necessary in order to obtain the maximum T_c-value.[3] The aim of this work was to study the damage production and the annealing behaviour in the Nb and in the C-sublattice separately by observing the yields of the Nb (α, α), Nb (d,d) elastic scattering and $^{12}C(d,p_0)^{13}C$ reactions in channeling effect studies.

Numerous channeling effect measurements have been performed in diatomic crystals[4] in order to test the channeling theories, which have been developed to describe the results for simple lattice structures. For diatomic lattices more complicated cases than in monoatomic structures exist, for example, parallel rows consisting of atoms A and B only and rows containing atoms A as well as atoms B and further rows with alternating spacings between atoms in the rows. In all these cases the results of the channeling measurements (the angular yield curves) can be described rather well by the continuum approximation where the nuclear and electronic charges are treated to be smeared out continuously along the row using average values for the spacings and for the atomic numbers.

For NbC single crystals in ⟨110⟩ direction it is expected[8] that the Nb—as well as the C-rows—reveal distinct critical angles and minimum yields that are described by theory within a few percent (a systematic deviation may exist for small impact parameters, see below). Stronger deviations in the angular yield curves for the Nb- or the C-rows in the NbC single crystals from the theoretical ones would indicate disorder in the sublattices. Any disorder analysis in implanted NbC single crystals requires a detailed knowledge of the angular yield curves for the undisturbed crystals. Therefore, prior to C-implantation detailed channeling studies have been performed on the $NbC_{0.89}$ single crystals and the results for the critical angle and the minimum yield have been compared with values obtained from several theoretical models.

EXPERIMENTAL

$NbC_{0.89}$ single crystals have been produced in a crystal-growing induction furnace by the zone floating technique under Ar pressure.[5] These crystals were implanted at 830°C with C^+ ions at energies of 200 and 80 keV and with fluences of 1.5×10^{17} cm^{-2} and 5×10^{16} cm^{-2}. After implantation the crystals were annealed at 1070 and 1190°C for 200 sec at each temperature in a bakeable UHV system.

The usual backscattering and channeling configuration has been used for analysis. The sample was mounted on a three axis goniometer and a solid

† Permanent address: Dept. of Physics, University of Pretoria, Pretoria, South Africa.

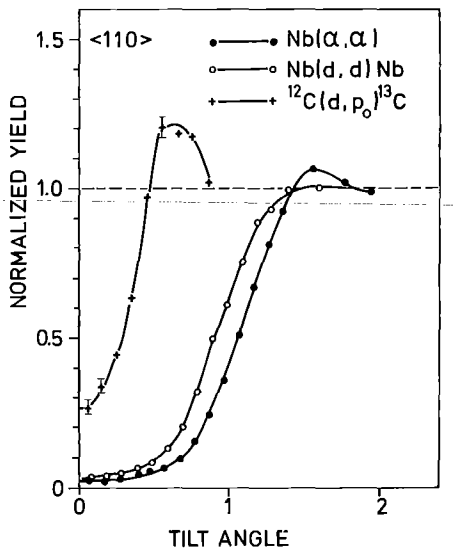

FIGURE 1 Normalized yields as a function of crystal orientation through the ⟨110⟩ axes. With the Nb (α,α) Nb and Nb (d,d) Nb-reactions the critical angles and minimum yields for the Nb-sublattice and with the $^{12}C(d,p_0)^{13}C$ the values for the C-sublattice of the NbC single crystal are measured.

state detector was placed at 165° in order to determine the energy of the reaction products. The angular spread of the incoming beam was less than 0.01°. In order to study simultaneously the niobium and carbon sublattices a 1.275 MeV deuteron beam has been used. With the ⟨110⟩ direction of the crystal aligned in the direction of the beam the rows of Nb-atoms could be studied with the elastically scattered deuterons and the carbon strings with the $^{12}C(d,p_0)^{13}C$-reaction. This reaction has a positive Q-value of 2.722 MeV and a relatively high differential cross section (100 mb/sterad) at energies near 1.2 MeV and at a laboratory angle of 165°.[6] The energy of 1.275 MeV has been chosen because the excitation curve shows a linear energy dependence between 1.2 and 1.275 MeV and the cross section is high in this energy region. The same detector has been used to measure both the elastic deuterons and the protons.

In the angular scan measurements two energy windows were used in both the elastic and reaction parts of the spectra. The two window settings in each case corresponded to two depth values near the surface as indicated by arrows in Figures 2 and 3 and the results obtained for the critical angle $\psi_{1/2}$

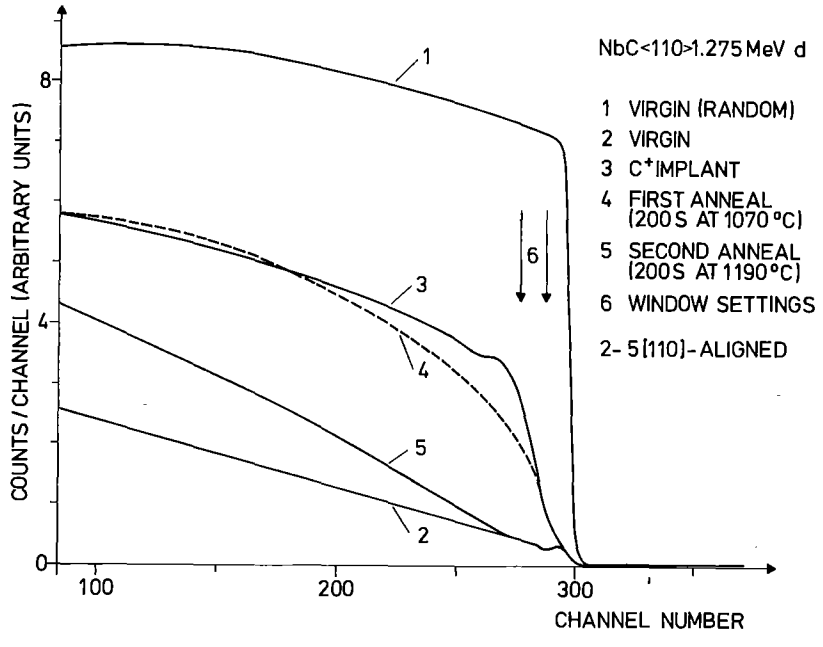

FIGURE 2 Random and ⟨110⟩ aligned energy spectra of 1.275 MeV deuterons elastically scattered from a NbC single crystal before and after C^+-implant and after two annealing stages ($\Theta = 165°$).

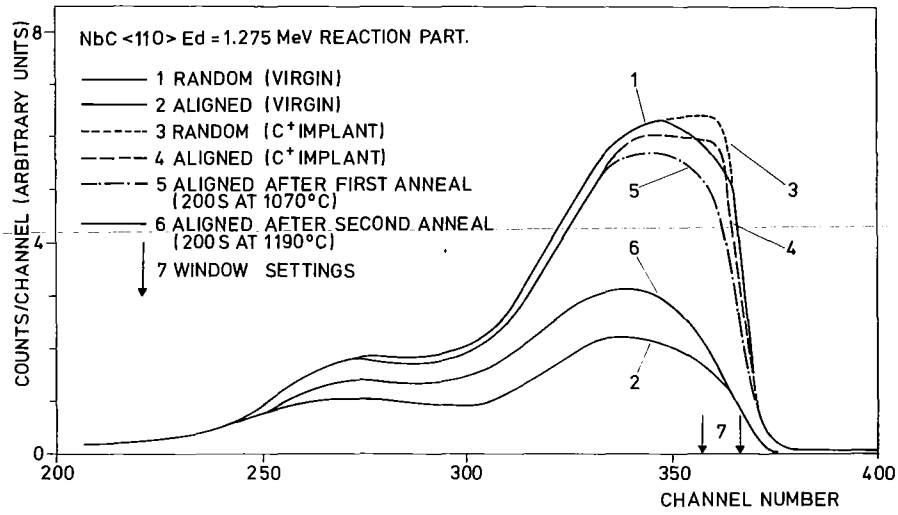

FIGURE 3 Random and ⟨110⟩ aligned energy spectra of protons emitted at 165° during the bombardment of a NbC single crystal with 1.275 MeV deuterons.

and the minimum yield χ_{min} have been extrapolated to the surface. In the angular yield curve $\psi_{1/2}$ is the half-angular width at half height between the minimum yield and the yield for a random direction; χ_{min} is the minimum yield normalized to the random yield. Care has been taken to use the same tilt plane in all the experiments.

In order to get more information on the damage structure in the Nb-sub-lattice measurements have also been performed at different incident energies of the ^{4}He ions.

RESULTS AND DISCUSSION

A Channeling Studies on $NbC_{0.89}$ Single Crystals Prior to C-implantation

Angular scan measurements have been performed through the [110] axial channel only. As an example, results of angular scans for He ions scattered from Nb, for deuterons scattered from Nb and for protons from the C(d,p) reaction are presented in Figure 1. The extrapolated values for $\psi_{1/2}$ and χ_{min} have been summarized in Tables I and II. The extrapolated values for $\psi_{1/2}$ are about 3% larger than the values measured for the scans near the surface, the extrapolated χ_{min} values are about 10% smaller.

The measured results for $\psi_{1/2}$ have been compared to values calculated with an empirical formula derived from Monte Carlo computer calculations:[7]

$$\psi_{1/2} = 0.8[V(1.2\,u_1)/E]^{1/2} \quad (1)$$

with $V(r) = E\psi_1^2 f(r/a)$ where $V(r)$ is the continuum potenial for a static row[7] with Molière's screening function $f(r/a)$.

$\psi_1 = (2Z_1Z_2e^2/dE)^{1/2}$ is the Lindhard characteristic angle,[8] where Z_1, Z_2 are the atomic numbers of the incoming and target atom, respectively, e the electronic charge, d the distance between the atoms

TABLE I

Measured $\psi_{1/2}$-values (extrapolated to zero depth) and $\psi_{1/2}^{cal}$-values calculated for various potentials

Reaction	$\psi_{1/2}^{extr.}$	$\psi_{1/2}^{cal}$ Barrett	$\psi_{1/2}^{cal}$ multi row pot. (Molière)	$\psi_{1/2}^{cal}$ multi row pot. (Lindhard)	$\psi_{1/2}^{cal}$ single row pot. (Lindhard)
Nb (α, α)	1.12 ± 0.03	0.95	0.93	0.99	0.99
Nb (d, d)	0.93 ± 0.03	0.85	0.83	0.87	0.89
C (d, p_0)	0.35 ± 0.03	0.37	0.36	0.38	0.4

TABLE II

Measured χ_{min}-values (extrapolated to zero depth) compared to calculated χ_{min}-values for [110] NbC

Reaction	$\chi_{min.}^{extr.}$	$\chi_{min.}^{cal.}$ [Eq. (2)]	$\chi_{min.}^{cal.}$ [Eq. (3)]	$\chi_{min.}^{cal.}$ [Eq. (4)]
Nb (α, α)	0.020 ± 0.003	0.031	0.02	0.017
Nb (d, d)	0.021 ± 0.003	0.031	0.02	0.017
C (d, p)	0.25	0.22	0.14	0.13

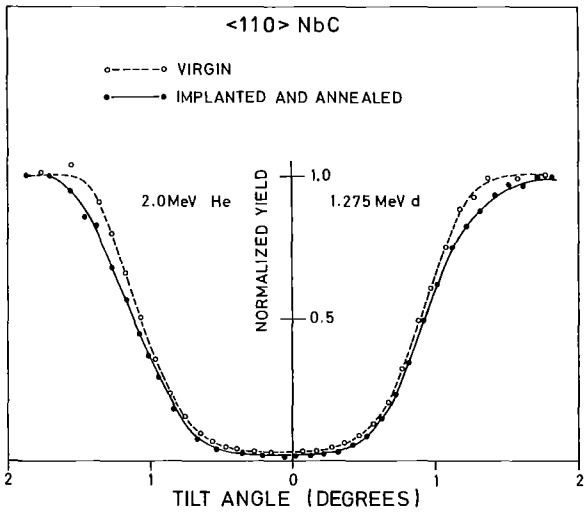

FIGURE 4 Yield as a function of orientation through the ⟨110⟩ axis of a NbC single crystal using 1.275 MeV deuterons and 2.0 MeV ^{4}He.

in the row and E the energy of the incoming particle. u_1 is the average thermal vibrational amplitude perpendicular to the row, $1.2 \times u_1$ is the distance of closest approach of channeled particles to the rows and a the Thomas Fermi screening parameter ($a = 0.4685 \times Z_2^{-1/3}$).

The u_1-values for the $NbC_{0.89}$ single crystals used in these experiments have been determined from the Debeye temperatures Θ_D of 390 K for the Nb sublattice and 1100 K for the C-sublattice evaluated from neutron scattering experiments.[9] From these Θ_D-values and assuming a Debye spectrum for the phonon density distribution the u_1-values have been found to be 0.063 Å for the C atoms and 0.057 Å for the Nb atoms. using these u_1-values the $\psi_{1/2}$-values have been calculated and the results are given in the third column in Table 1. A reasonable agreement exists between the measured and calculated $\psi_{1/2}$-values for the C rows; however, one should note that the error bars are relatively large in this case. For the Nb rows the $\psi_{1/2}^{exp}$ values are substantially larger than the calculated values. This discrepancy seems to be of principle nature as is discussed in the following:

Equation (1) has been set up for protons incident on tungsten and the $\psi_{1/2}$-values calculated from this equation for a great variety of targets, ion-beam species, energies and orientations agree with measured values to within 5 to 10%. A detailed comparison[10] however showed that the measured values are systematically larger for small impact parameters ($\sqrt{2}u_1/a \lesssim 0.7$). This condition is fulfilled for the Nb rows (0.59) as well as for the C rows (0.24) in NbC. Therefore our results for the Nb rows are in agreement with this general observation. For the C rows in addition one has to consider the influence of the Nb row potential on the $\psi_{1/2}$-values of the C-row. Therefore the potential-energy contour diagram for the ⟨110⟩ direction in NbC has been determined using the continuum potential with Lindhard's as well as with Molière's screening function and considering the potential contribution from a matrix of 6 × 8 atoms in the calculation. From this calculation the multirow potential $\sum V(1.2u_1)$ and V_0, the minimum potential in the open channels between the rows have been determined and the $\psi_{1/2}$-values have been calculated by inserting $V(1.2u_1) = \sum V(1.2u_1) - V_0$ in Eq. (1) following the procedure described in Ref. 11. These $\psi_{1/2}$-values are also presented in Table I, columns 4 and 5. The multi-row potential with Molière's screening function yield somewhat smaller $\psi_{1/2}$-values as obtained from Barrett's formula. Better agreement with the measured values is obtained by using the multi-row potential with Lindhard's screening function. The influence of the Nb row potential on the $\psi_{1/2}$-values for the C-rows is small as can be judged by comparing the $\psi_{1/2}$-values in columns 5 and 6.

The second parameter used for comparison between theory and experiment is the minimum

yield. Several possibilities exist in calculating the χ_{min} values for polyatomic crystals. Firstly, the geometrical model,[8] $\chi_{min} = \pi Nd(2u_1^2 + a^2)$, may be used or the equation derived from Monte Carlo calculations:[7]

$\chi_{min} = 3\pi Nd2u_1^2$ where N is the density of target atoms and $\sqrt{3}\cdot\sqrt{2}\cdot u_1$ is interpreted as follows:[11] particles incident parallel to the row with impact parameters smaller or equal to $\sqrt{3}\cdot\sqrt{2}\cdot u_1$ will be dechanneled and will then contribute to the minimum yield. Secondly, the contribution of the atom B rows to χ_{min} of the atom A rows and vice versa may be estimated in two different ways:

i) Contributions from B rows to χ^A_{min} of A rows may be treated by multiplying χ^B_{min} with a factor K,[12] which is proportional to the relative scattering power from the rows. For the geometrical model follows:

$$\chi^A_{min} = [\pi Nd(2u_1^2 + a^2)]_A + K[\pi Nd(3u_1^2 + a^2)]_B. \quad (2)$$

For the computer model in a similar way:

$$\chi^A_{min} = (18.8\ Nd\ u_1^2)_A + K(18.8\ Nd\ u_1^2)_B. \quad (3)$$

K can be estimated from the continuum potential to be $Z_B d_A / Z_A d_B$ ($d_A = d_B = 3.161$ Å for NbC).

ii) The contribution from B rows to χ^A_{min} of the A rows may also be calculated by the procedure given in Ref. 11:

$$\chi^A_{min} = (18.6\ Nd\ u_1^2)_A + (\pi\ Nd\ r_c^2)_B. \quad (4)$$

r_c is determined from $V^B(r_c) = V^A(6u_1^A) - V_0$, where V^A is the potential of the A rows with the impact parameter $\sqrt{2}\cdot\sqrt{3}\cdot u_1^A$ as defined before. For Nb atoms as A rows the contribution of the second terms in Eqs. (3) and (4) is only about 10% to χ^A_{min}, however for C as A rows the contribution is about 80%.

χ_{min}-values have been calculated from Eqs. (2), (3) and (4) and the results are presented in Table II. For the Nb rows the χ_{min} values calculated from Eq. (2) are found to be larger than the experimental values. This is due to the fact that the a-values are larger than the u_1-values. χ_{min}-values obtained from Eqs. (3) and (4) are very similar and no decision between both models can be made. The relatively large χ_{min}-values for the C-rows are due to strong contributions from the Nb-rows steering deuterons with deflection angles $\psi_{1/2}$ into the C-rows. Nevertheless the calculated values are considerably smaller than the measured values. This result may indicate that some defects exist in the C-sublattice. The reason for this discrepancy may also be partly explained by uncertainties in using the zero depth extrapolating process for nuclear reactions. Although the calculated χ_{min}-values for the Nb-rows are smaller than the experimental values the agreement is reasonably good. In general, the model that gives the smallest χ_{min}-value should be favoured as some contribution to χ_{min} from amorphous layers may be expected. The contribution χ_3 from n_s amorphous layers has been calculated using:[8]

$$\chi_3 = \sum_s n_s \frac{\pi}{4} Nd^3 \frac{\Psi_1^4}{\chi^2_{1/2}}$$

where the sum extends over the atomic species s. From this calculation follows that $\chi_3 = 0.001$ for one amorphous monolayer NbC. From the area of the Nb surface peak in the aligned elastic backscattering spectra two monolayers have been calculated. The good agreement between calculated and measured $\psi_{1/2}$- and χ_{min}-values indicate a damage-free Nb sublattice whereas the deviations observed for the χ_{min}-values of the C-rows may be due to damage in the C sublattice.

B Channeling Studies in C-implanted $NbC_{0.89}$ Single Crystals

The channeling studies described in this chapter are closely related to results[3] from similar C-implanted single crystals, where T_c has been measured as a function of implantation and annealing temperature. From these previous studies it is known that T_c increases from 4 to 11 K after C-implantation at 830°C, a further increase to 11.5 K is observed after additional annealing at 1070°C and is not affected during further annealing up to 1190°C.

The purpose of the following work is to determine the radiation induced disorder in the C-sublattice for these various implantation and annealing temperatures. Implantation of 5×10^{16} C/cm^2 at 80 keV and 1.5×10^{17} C/cm^2 at 200 keV, corresponding to an amount of about 12% over a depth of 3000 Å, have been performed at 825°C. Backscattering and reaction spectra for the random oriented and ⟨110⟩ aligned crystal have been taken after implantation and after annealing at 1070°C and at 1190°C for 200 sec. The spectra taken at the different annealing stages are presented in Figure 2 for the Nb (d,d) elastic part and in Figure 3 for the reaction part. The shape of the spectra in Figure 3 resembles the reaction cross section as a function of energy; the

depth corresponding to the width of the peak at high energies is about 8000 Å. In contrast to previous work[13] where the amount of implanted C could be determined from a drop in the yield of the random spectrum from He ions backscattered from Nb atoms, the amount of implanted C can be estimated from the difference in yield of the random spectrum prior and after C-implantation (spectrum 1 and 3 in Figure 3).

A remarkable difference can be seen in comparing the dechanneling yield defined as the ratio of the yield in the aligned spectra minus the yield in the aligned spectra of the virgin crystal to the yield of the random spectra in the Nb- and in the C-sublattice. The dechanneling yield for the Nb-sublattice increases steeply with depth and is about 0.25 at half height and saturates at 0.39, whereas for the C-sublattice the dechanneling yield is about 0.75 in the implanted region. As the dechanneling yield is proportional to the amount of damage present it is concluded that there is more damage in the C-sublattice than in the Nb-sublattice. Indeed it has been shown previously[3] that annealing of Nb atoms in NbC displaced during implantation at room temperature, has already occurred for implants at 830°C. The shape of the dechanneling curve for the Nb sublattice after C implantation at 830°C indicates that the damage is not due to single defects but rather to extended defects such as stacking faults and dislocations for example.

In order to get more information on the kind of damage that prevails in the Nb sublattice after C implantation at 830°C the energy of the He beam has been varied between 1 and 2.8 MeV. It is known[14] that from the energy dependence of the dechanneling yield some conclusions can be drawn on the type of defects. The dechanneling yield as a function of depth has been measured at 1.0, 2.0 and 2.8 MeV. No energy dependence could be observed and this excludes simple one-dimensional defects such as point defects or dislocations and can be explained by stacking faults. These extended damage componenets will contribute to the dechanneling yield of the Nb as well as of the C sublattice.

For the annealing stages at 1070 and 1190°C the recovery of the Nb-sublattice and the C sublattice occurs at the same time. The dechanneling yield after annealing at 1070°C is about 0.55 for the C sublattice and 0.20 for the Nb sublattice, at 1190°C the recovery is nearly completed with about 0.09 dechanneling yield in the C-sublattice and 0.04 in the Nb-sublattice near the surface.

Angular scan measurements have been performed after the various annealing stages given above. In contrast to the results from the undisturbed crystal $\psi_{1/2}$ was found to increase with depth for the damaged crystal. This effect is probably due to the steep rise in χ_{min} with depth as the $\psi_{1/2}$-values are determined by definition at height $(1 - \chi_{min})/2$. The $\psi_{1/2}^{exp}$-values for the damage were found to be slightly larger than those obtained for the undisturbed crystal. The results for the extrapolated values $\psi_{1/2}$ and χ_{min} after different annealing stages are summarized in Table III. The angular scan curve obtained for the Nb (α,α) and Nb (d,d) elastic scattering after annealing at 1190°C have been compared in Figure 3 to the angular scan curve obtained from the crystal after the implanted layer had been lapped off and the crystal had been re-etched. The smaller $\psi_{1/2}$-value observed for the re-etched crystal is in agreement with the $\psi_{1/2}$-value obtained prior to implantation for the undisturbed crystal. This result may be explained by a small increase of the Debye temperature Θ_D in the implanted layer of about 100 ± 50 K. As it is known from specific heat measurements[15] that Θ_D increases by about 50 K with increasing C-content from 0.89 to 0.98 this seems to be a reasonable explanation for the observed effect.

The main results and conclusions of this work may be summarized as follows:

i) The critical angle of Nb rows in [110]-NbC is larger than that calculated by Eq. (1) using several potentials, but is in agreement with a general trend for experimental data summarized in Ref. 10. For reduced impact parameters $\sqrt{2}u_1/a$ from the row equal or smaller as about 0.7 the continuum potential with Lindhard's screening function provides the best agreement with the measured $\psi_{1/2}$-values. Using multi-row potentials will lead to a small decrease in the calculated $\psi_{1/2}$-values. The calculation indicates that the Nb row potential will reduce the $\psi_{1/2}$-values for the C rows by about 0.02°.

TABLE III

$\chi_{1/2}$ and χ_{min} values for [110] NbC extrapolated to zero to zero depth after various annealing stages

Reaction	T_A, T_1	$\psi_{1/2}^{extr.}$	$\chi_{min}^{extr.}$
Nb (d, d)	$T_1 = 830$°C	0.97	0.1
Nb (d, d)	$T_A = 1070$°C	0.99	0.11
Nb (d, d)	$T_A = 1190$°C	0.97	0.027
Nb (α, α)	$T_A = 1190$°C	1.16	0.017
Nb (d, p)	$T_A = 1190$°C	0.35	0.26

ii) According to our results in calculating χ_{min}-values the computer model should be used as the χ_{min}-values given by the geometrical model are larger than the experimental values. In calculating the contributions from the B rows to χ_{min} of the A rows and vice versa Eq. (4) should be used as it provides the smallest χ_{min}-value of 0.017 in agreement with experimental value given in Table III.

iii) From the dechanneling yields in C-implanted NbC single crystals it is concluded that the amount of damage in the C-sublattice is larger than in the Nb-sublattice. The energy independence of the dechanneling yield for Nb-sublattice is attributed to the existence of extended defects such as stacking faults and equal contributions from these kinds of defects to χ_{min} of both sublattices are expected. The enhanced dechanneling yield observed for the C-sublattice may be due to C-precipitations. As T_c increases from 4 to about 10.5 K during C-implantation at 825°C, it is concluded that T_c of NbC is rather insensitive to the presence of this extended defects. The insensitivity of this material to radiation damage has been shown previously for Ar-bombarded NbC thin films.[16] Additional annealing at 1190°C will drastically lower the dechanneling yield from 0.4 to 0.04 for the Nb sublattice and from 0.75 to 0.09 for the C sublattice. The T_c increase from about 10.5 to 11.5 K observed for this annealing step is however small.[17]

ACKNOWLEDGEMENTS

The authors wish to thank Dr. J. Geerk and G. Linker for valuable discussions, M. Kraatz for performing the C-implantations and R. Kaufmann fro providing the program on multi-row potential calculations. One of us (J.M.L.) acknowledges financial support from the Council of Scientific and Industrial Research in South Africa.

REFERENCES

1. A review and summary on superconducting properties of refractory material is given in L. E. Toth: *Transition Carbides and Nitrides* (Academic Press, New York and London).
2. A. L. Giorgi, E. G. Szklarz, E. K. Storms, A. L. Bowman and B. T. Matthias, *Phys. Rev.* **125**, 837 (1962).
3. J. Geerk and K. G. Langguth, *Solid State Com.* **23**, 83 (1977).
4. A review of the channeling technique and a summary of references on channeling in non-simple crystals is given by D. S. Gemmell, *Rev. Mod. Phys.* **46**, no. 1 (1974).
5. B. Scheerer and W. Reichardt, Progress Report of the IAK I, Ges. für Kernforschung mbH, Karlsruhe, KFK 2357, edited by W. Schommers (1974), 74.
6. M. Huez, L. Quaglia and G. Weber, *Nuclear Instruments and Methods*, **105**, 197 (1972).
7. J. H. Barrett, *Phys. rev.* **B3**, 1527 (1971).
8. J. Lindhard, *Kgl. Danske Videnskab. Selskab. Mat.-Fys. Medd.* **34**, no. 14 (1965).
9. F. Gompf, L. Pintschovius, W. Reichardt and B. Scheerer, *Proc. of the Conf. on Neutron Scattering, Gatlinburg*, June 6–10, 1976, Vol. I, p. 129, and W. Reichardt, private communication.
10. J. U. Andersen and E. Laegsgård, *Rad. Effects*, **12**, 3 (1972).
11. D. S. Gemmell and R. L. Mikkelson, *Rad. Effects*, **12**, 21 (1972).
12. L. Eriksson and J. A. Davies, *Ark. Fys.* **36**, 439 (1969).
13. K. G. Langguth, G. Linker and J. Geerk, *Ion Beam Surface Layer Analysis*, edited by O. Meyer, G. Linker and F. Käppeler (Plenum Press, 1976).
14. Y. Quéré, *Rad. Effects*, **28**, 253 (1976).
15. L. E. Toth, M. Ishikawa and Y. A. Chang, *Acta. Met.* **16**, 1183 (1968).
16. O. Meyer, H. Mann and E. Phrilingos, *Application of Ion Beams to Materials*, edited by S. T. Picraux, E. P. EerNisse and F. L. Vook (Plenum Press, New York, 1974).
17. J. Geerk, K. G. Langguth, G. Linker and O. Meyer, *I.E.E.E. Transactions on Magnetic*, Vol. MAG-13, no. 1, Jan. 1977, p. 662.

Journal of Nuclear Materials 72 (1978) 182–189

RADIATION DAMAGE AND SUPERCONDUCTIVITY IN V_3Si SINGLE CRYSTALS

O. MEYER

Kernforschungszentrum Karlsruhe, Institut für Angewandte Kernphysik, D-7500 Karlsruhe, Postfach 3640, Fed. Rep. Germany

Single crystals of V_3Si have been implanted at room temperature with Zr, Kr and He ions and were analysed using the backscattering and channeling techniques. A strong component of direct backscattering has been observed due to randomly displaced interstitials resulting in amorphization at Kr ion fluences of about $3 \times 10^{14}/cm^2$, similar to those observed for covalently bonded systems. For He ions, using the same energy-deposited density, this component is found to be a factor of about 30 lower than that observed for heavy ions. In the region of low damage level (near the surface) for crystals implanted with 300 keV He ions a narrowing of the critical angle of about 12% is found for the [100] as well as for the [110] channeling direction. These results can be explained assuming the V-atoms have been displaced from their lattice sites with an average displacement of about 0.1 Å. The influence of the various damage structures on the superconducting transition temperature T_c is discussed.

Des monocristaux de V_3Si ont subi l'implantation à la température ambiante d'ions Zr, Kr et He puis ont été analysés en utilisant les techniques de rétrodiffusion et de canalisation. Une composante intense de rétrodiffusion a été observée qui est due à des interstitiels déplacés au hasard, ce qui provoque une amorphisation pour des fluences d'ions Kr de $3 \times 10^{14}/cm^2$, semblable à celle observée pour les systèmes à liaison covalente. Pour les ions He, en utilisant la même densité d'énergie déposée, cette composante s'est révélée être inférieure d'un facteur 30 environ à celle observée pour les ions lourds. Dans la région à fiable degré de dommages (proche de la surface) pour des cristaux implantés avec des ions He de 300 keV un rétrécissement de l'angle critique d'environ 12% a été trouvé pour la direction de canalisation [100] ainsi que pour la direction [110]. Ces résultats peuvent être expliqués en supposant que les atomes de vanadium ont été déplacés de leurs sites réticulaires, le déplacement moyen étant de 0.1 Å environ. L'influence de diverses structures de dommages sur la température de transition de supraconductibilité T_c est discutée.

V_3Si-Einkristalle wurden bei Raumtemperatur mit Zr-, Kr- und He-Ionen implantiert und mit Hilfe der Channelling- und Rückstreutechnik analysiert. Eine starke direkte Rückstreukomponente von regellos verteilten Atomen wurde beobachtet, die bei einer Kr-Fluenz von 3×10^{14} cm^{-2}, ähnlich, wie bei kovalent gebundenen Systemen, zu einem völlig gestörten Zustand führt. Für He-Ionen ist bei gleicher übertragener Energiedichte diese Komponente etwa 13mal kleiner als für schwere Ionen. Im Bereich kleiner Strahlenschädigung (nahe der Oberfläche) werden nach Implantation von 300 keV-He-Ionen ein Anwachsen der minimalen Ausbeute und eine Verengung des kritischen Winkels um etwa 12% sowohl für die [100]-als auch für die [110]-Channellingrichtung beobachtet. Diese Ergebnisse lassen sich durch die Annahme einer statistischen Verlagerung der V-Atome von ihren Gitterplätzen mit einer mittleren Verlagerungsamplitude von etwa 0,1 Å erklären. Der Einfluss der verschiedenen Schädigungsstrukturen auf die Übergangstemperatur zur Supraleitung wird diskutiert.

1. Introduction

V_3Si is one of the well-known superconducting compounds with the A15 structure. In this class of materials T_c is related to the linear chains of the transition metal atoms. A large depression of T_c has been observed after irradiation with neutrons [1], heavy ions [2,3] and light ions [4]. The mechanism responsible for the radiation-induced reduction in T_c appears to be similar [4]. Several models have been discussed in the literature. However the crucial question of what kind of damage structure causes the T_c depression still remains unsolved. From X-ray diffraction results it has been concluded that irradiation produces an exchange of atoms between the atomic sites (antisite defects) thus reducing the Bragg–Williams long range order parameter [5] which is related to T_c [6]. Furthermore, T_c may be lowered because of the proximity effect due to the presence of disordered regions having no or low T_c-

value [7]. The T_c degradation by irradiation is also thought to be due to the reduction of the density of electronic states caused by electron scattering on defects of unknown structure [8]. The purpose of this study is to use channeling and backscattering of He ions in damaged V_3Si single crystals in order to get some insight into the structure of the damage present.

The backscattering and channeling techniques have been successfully used for investigations of damage distributions in semiconductors [9] and metals [10, 11]. As point defect agglomerates are the most stable defect structures after irradiation in metals, a direct backscattering component from interstitials or atoms, displaced more than 0.2 Å from their lattice site plays a minor role. These extended defects will increase the transverse energy of the incident particle beam and thus deflect particles from channeled to random trajectories. This dechanneling process will mainly be caused by the large strain fields connected with the point defect clusters [10]. The dependence of the dechanneling yield on the analysing beam energy will provide further information on the nature of extended defects (dislocations, voids, stacking-faults etc.) [12]. The transverse energy of the analysing beam can also be varied by changing the angle of incidence through channeling directions. Angular scan curves were measured in order to study damage structures where many atoms are displaced from their lattice sites by small amounts (<0.2 Å) [13].

2. Experimental technique

A V_3Si single crystal [14] was cut almost perpendicular to the crystallographic [100] and [110] directions on opposite sides. Surfaces were lapped and polished with diamond paste and etched in a 4 : 1 : 1 mixture of H_2O : HF : H_2O_2. Implantations were performed off-axis at room temperature over the whole sample surface using a scanned ion beam from a 400 keV implantation machine. A bakeable UHV–system with an electron beam oven was used for crystal annealing. The usual backscattering and channeling configuration has been used. The sample was mounted on a three-axis-goniometer and a solid state detector was placed at 165° in order to determine the energy and yield of the backscattered He–particles. Particles elastically scattered from the V-atoms were well separated in energy from those scattered from Si-atoms. During angular scan measurements the low index channeling directions were tilted through the analysing beam direction and the backscattered particle yield was registered. The minimum yield χ_{min} is the aligned yield normalized to the random yield and $\psi_{1/2}$, the critical angle, is the half-angular width at half height between the minimum yield and random yield.

3. Analysis

As has been shown previously [9], backscattering spectra of light ions from random or channeled directions can be analysed to yield information on the amount of damage produced during irradiation. Information can also be obtained on the depth distribution and masses of impurities near the surface which are heavier than the host material. Typical spectra from 2 MeV He ions backscattered from V_sSi for random and [100] aligned incidence prior to and after implantation of 10^{16} Zr^+/cm^2 at 140 keV and after annealing at 920°C are presented in fig. 1. The random spectrum reveals two steps from He-ions backscattered from V-atoms and from Si-atoms (lower energy). The [100] aligned spectrum shows three small peaks from displaced V and Si, and O-atoms forming a natural oxide layer on the lapped

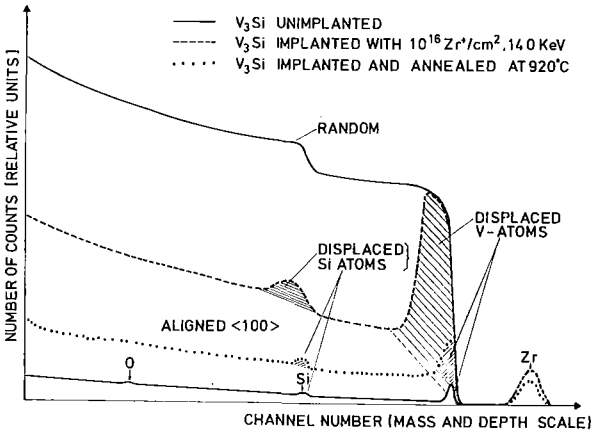

Fig. 1. Backscattering spectra for random and [100] aligned He-ion incident on a V_3Si single crystal prior to and after implantation of 10^{16} Zr^+/cm^2 at 140 keV and after additional annealing at 920°C.

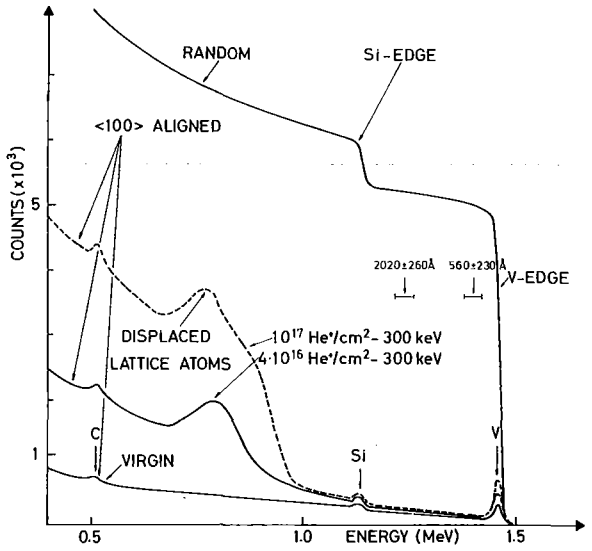

Fig. 2. Backscattering spectra for single crystal V_3Si implanted with large He fluences (4×10^{16} He^+/cm^2 and 10^{17} He^+/cm^2) at 300 keV. The disorder peak is shifted to a depth of approximately 6000 Å. A small enhanced dechanneling yield is observed in the surface region where the angular scan measurements were performed (window settings are indicated.

and etched surface. After implantation of Zr-ions three large peaks are visible in the aligned spectra due to Zr atoms, displaced V-atoms and displaced Si-atoms. From the peak areas, the number of implanted Zr/cm^2 and the number of displaced V- and Si-atoms can be calculated [15]. The accuracy in the determination of the damage peak areas is limited by uncertainties in background subtraction.

After implantation of 300 keV He^4-ions the damage level near the surface is low and only a small dechanneling component can be observed (fig. 2). This kind of depth dependence of the dechanneling yield is usually found for metals and has been correlated with the appearance of point defect agglomerates [10]. In that detailed study using single crystal Au foils, dechanneling and TEM results on visible clusters have been combined and a dechanneling cross section σ_d equal to 2.3×10^{-14} cm^2 has been obtained [10]. From the dechanneled fractions χ_{min} and $\chi(z)$, before and after damage respectively, the density of visible clusters N_s may be estimated from:

$$N_s = \Delta(d\chi/dz)/[(1 - \chi_{min}) \cdot \sigma_d] \,. \qquad (1)$$

For an estimate of the amount of energy deposited by nuclear collisions E_n, the power approximate to the reduced differential cross section for the Thomas–Fermi potential was used applying a useful interpolation formula [16]. The average number of Frenkel pairs N_v is, as usual, estimated to be $N_v = E_n/2\,E_{eff}$, where E_{eff} is an effective displacement threshold energy.

The measured results for $\psi_{1/2}$ have been compared to values, calculated with an empirical formula derived from Monte Carlo computer calculations [17]:

$$\psi_{1/2} = 0.8[V(1.2 \times u_1)/E]^{1/2} \,, \qquad (2)$$

with $V(r) = E \times \psi_1^2 \times f(r/a)$ where $V(r)$ is the continuum potential for a static row with Molière's screening function $f(r/a)$. ψ_1 is the Lindhard characteristic angle [18]. u_1 is the average thermal vibrational amplitude perpendicular to the rwo, $1.2 \times u_1$ is the distance of closest approach of channeled particles to the rows and a ($a = 0.4685 \times Z_2^{-1/3}$) the Thomas–Fermi screening parameter.

Following the procedure of Pande [7], the T_c depression due to the proximity effect has been calculated. The calculation is based on the BCS theory: $T_c \simeq \theta_b \exp - [1/(N(0)V)]$ with an effective $(N(0)V)_{eff}$-value derived by DeGennes [19] for a layered structure:

$$[NV]_{eff} = (N_n^2\, V_n d_n + N_s^2\, V_s d_s)/(N_n d_n + N_s d_s) \,, \qquad (3)$$

where d_s and d_n are the thicknesses of the superconducting and normal conducting (or lower T_c) films, respectively. Combining the T_c-formula for the bulk material and for the composite structure one obtains:

$$T_c = T_{c0} \exp\{N_n V_n N_s V_s/(N_s V_s - N_n V_n)$$

$$+ N_s V_s (N_s/N_n)(d_s/d_n)/(N_s V_s - N_n V_n)\} \,, \qquad (4)$$

where the ratio d_s/d_n is replaced by $\langle d\rangle/r$, $\langle d\rangle$ is the average mean free distance between spherical disordered regions of radius r. Bansal and Ardell [20] calculated the dependence of $\langle d\rangle/r$ on F, the disordered volume fraction. This function has to be modified and is extrapolated to $F = 0.64$ (random dense packing of spheres) for $\langle d\rangle/r$-values smaller than 0.3. The fraction of disordered regions is calculated by $F = 1 - \exp(-V_d n_p)$, where V_d is the volume of a disordered region and n_p the density of primary knock on particles producing such a region ($n_p \sim$ fluence).

4. Results

4.1. Heavy ion radiation damage

The damage contribution to well resolved peaks as shown in fig. 1.consists of V- and Si-atoms, displaced more than about 0.2 Å from their lattice sites. If the damage peak touches the random level, the structure has been rendered amorphous as has been shown for Si [9]. A well resolved damage peak is also found due to polycrystalline layer formation by strain release for high fluence implantation in V [11]. In order to avoid this situation small fluences of Kr-ions at 50 keV were implanted in V_3Si and the relative damage peak area for V as a function of Kr-ion fluence is shown in fig. 3. For Kr fluences equal or above $3 \times 10^{14}/cm^2$, corresponding to a concentration of 0.3 at.%, the damage peak reaches the random level and saturates. The lower sensitivity limit is given by the surface peak prior to implantation. This peak stems from the surface V-atoms and from atoms displaced by oxide formation at the surface. About 10 monolayers of V_3Si are displaced as evaluated from the surface peak area. Assuming that the number of scattering centers contributing to the peak areas are equal to the number of displaced atoms it is found that about 720 V-atoms and 260 Si-atoms have been displaced by one Kr-ion at 50 keV. The number of displaced Si-atoms is about 1/3 of the displaced V-atoms.

From theory as outlined above it is estimated that about 45 keV of the total Kr ion energy is transferred into nuclear collisions. Together with the number of displaced V-atoms an effective displacement threshold energy of 23 eV is estimated and a similar threshold energy is observed for the Si atoms. The fluence of 3×10^{14} Kr/cm^2 for saturation corresponds to about 2.4 dpa (displacements per atom), indicating that annealing or recombination effects are small.

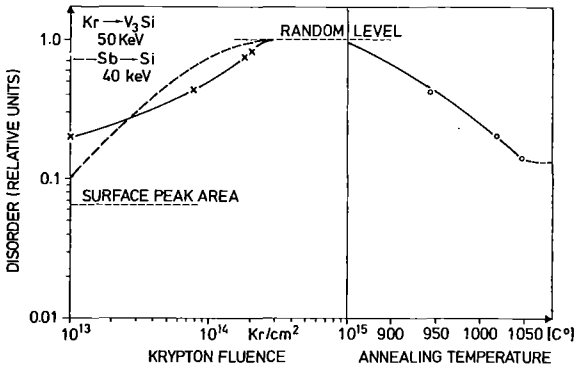

Fig. 3. Normalized damage peak area as function of the Kr-ion fluence and of the annealing temperature. For comparison the damage dependence on heavy ion fluence in Si is included (dashed line) [9].

The results presented in fig. 3 are compared to those which were obtained for 50 keV Sb ions implanted in Si (dashed line in fig. 2) [9]. A remarkable agreement exists for the damage production in the semiconductor Si and in the metal V_3Si. As current models for displacement processes in metals and semiconductors are substantially different from each other, one may conclude that the type of bonding in V_3Si is different from other metals and that a large component of covalent bonding exists. Strong covalent bonding between adjacent V-atoms in V_3Si has indeed been observed by X-ray diffraction [21]. The disorder peaks anneal at temperatures above 900°C as shown in fig. 3. At temperatures above 1000°C an enhanced surface peak remains, possibly caused by an oxide layer of increased thickness.

4.2. Light ion radiation damage

Light ions with energies above a few hundred keV will penetrate the surface region with little energy loss and will produce displacements at the end of their range. This latter part of the damage profile has been simulated by implanting He-ions to a fluence of $1.8 \times 10^{16}/cm^2$ at 50 keV. The backscattering spectrum is compared in fig. 4 with the result obtained by implanting 2×10^{14}Kr/cm^2 at 50 keV. From the damage peak areas, which are nearly equal, it is found that about the same number of displaced V-atoms/cm^2 have been produced although the number of implanted He-ions/cm^2 is a factor of 75 larger than the implanted number of Kr-ions/cm^2. After correcting for the amount of energy transferred by nuclear collisions the damage produced by the Kr-ions is about a factor of 13 larger than that for He-ions. This disagreement between retained damage after light and heavy ion irradiation has also been observed for Si where the retained damage could further be enhanced by using polyatomic ion implantation [22]. It is believed that

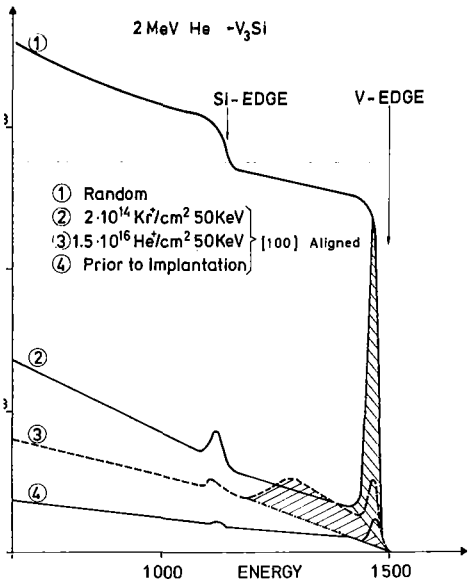

Fig. 4. Backscattering spectra for single crystal V_3Si implanted with 2×10^{14} Kr^+/cm^2 at 50 keV and 1.5×10^{16} He^+/cm^2 at 50 keV. Disorder peak areas (dashed) are nearly equal.

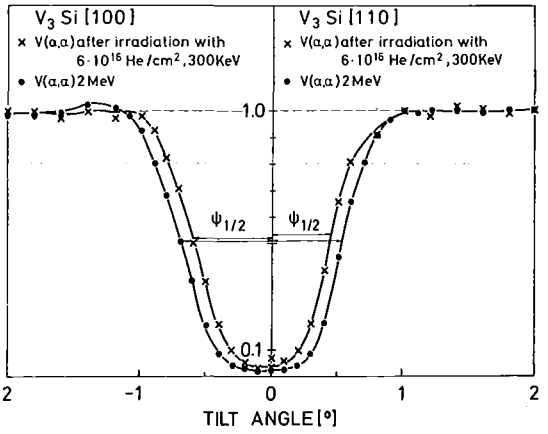

Fig. 5. Angular scan curves from 2 MEV He ions scattered from V in V_3Si single crystal for the [100] and the [110] axes prior to an after implantation of 6×10^{16} He/cm^2 at 300 keV.

the deposited energy density within each individual collision cascade will determine how much damage is created and retained. It follows that the effective displacement energy for He-ions implanted into V_3Si at RT is about 300 eV. Recent measurements [22] have shown that the damage area increases if larger transverse energy is used in the channeling analysis, indicating additional displacements with small amplitudes.

When increasing the implanted He-ion energy up to 300 keV the particles will penetrate a surface region of about 3000 Å with low energy loss. This effect can be seen in fig. 2 where the damage distribution is evident from the channeled spectra. The He-particles are stopped at a depth of approximately 6000 Å, where a peak from displaced lattice atoms is visible. In the region of interest however, the first 3000 Å below the surface, only a small increase in the dechanneling yield can be seen, which may be due to the existence of extended defects [10]. The density of clusters N_s is estimated from the depth dependence of dechanneling to be about $10^{17}/cm^3$ using eq. 4.

In order to look for different damage structures in the region of low damage level near the surface, angular scan measurements have been performed [27] at the depths as indicated in fig. 2. The angular yield curves prior and after implantation of 6×10^{16} He/cm^2 are shown in fig. 5 for the [100] as well as for the [110] channeling direction. An appreciable narrowing of the $\psi_{1/2}$-values and a slight increase in χ_{min} can be seen. This result has been verified in a total of 8 implants, as a function of fluence and

Table 1.
Measured $\psi_{1/2}$- and χ_{min}-values after irradiation with 6×10^{16} He/cm^2. The $\langle u \rangle$-values have been calculated by eq. 4, using $\psi_{1/2}^{exp}$ and $\Sigma V(1.2\,u) - V_0$. Values prior to irradiation are given in brackets.

Experiment	$\psi_{1/2}^{exp}$ (°)	$\langle u \rangle$(Å)	χ_{min}^{exp}	χ_{min}^{cal}
$V(\alpha, \alpha)$ [100] 2 MeV	0.68 (0.75)	0.104 (0.084)	0.034 (0.018)	0.07 (0.034)
$V(\alpha, \alpha)$[110] 2 MeV	0.44 (0.52)	0.086 (0.05)	0.065 (0.02)	0.08 (0.020)

Table 2.
Values of $\psi_{1/2}$ and χ_{min} at zero target thickness as a function of He fluence (300 keV), lowering of T_c as a function of He fluence (2 MeV) as determined by Poate et al. [4].

Fluence at 2 MeV [4] ($\times 10^{17}$)	Corresponding fluence at 300 keV ($\times 10^{16}$)	Average T_c(K) [4]	$\psi_{1/2}$	χ_{min}
–	–	16.4	0.75 ± 0.01	0.020
0.6	0.9	12	0.75	0.022
1.3	0.2	7	0.72	0.028
2.6	0.4	3.5	0.70	0.03
0.4	0.6	2.5	0.67	0.032
6.6	10	2.5	0.68	0.04
0.8	12	–	0.67	0.032

using a second V_3Si crystal cut perpendicular to the [110] direction. The measured results for $\psi_{1/2}$ and χ_{min} are summarized in table 1 and have been compared to calculated values [24]. The mean vibration amplitude calculated from eq. 5 (by inserting $\psi_{1/2}^{exp}$ and the multi-row potential) strongly increases after implantation of 6×10^{16} He/cm^2 at 300 keV. The experiment can not decide presently if this large displacement is of statical or dynamical nature. It is unrealistic however to assume an increase of the thermal vibration amplitude by such an amount. As the $\langle u \rangle$-values increase after implantation, it is expected that the χ_{min}-values would also increase in agreement with the experiment.

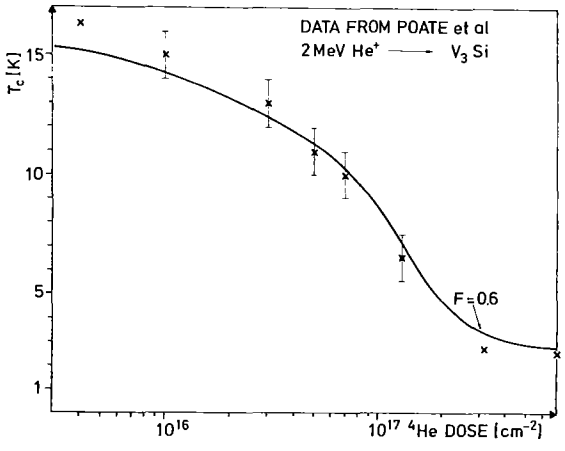

Fig. 6. Decrease of T_c with implanted He fluence as measured on irradiated V_3Si thin films [4] and compared to calculations using the proximity effect with the ratio N_s/N_n and the relative disturbed volume F as fit parameters.

The narrowing of $\psi_{1/2}$ and the increase of χ_{min} is measured as a function of the implanted He-ion fluence and the results are presented in table 2. The narrowing of $\psi_{1/2}$ and an increase of χ_{min} occurs for fluences above 6×10^{16} He/cm^2. As the T_c degradation in the implanted layer on bulk V_3Si single crystals can not be measured, the values of T_c for V_3Si thin films as a function of He-fluence as measured by Poate et al. [4] have been taken (fig. 6) and will be related to the observed decrease in $\psi_{1/2}$ and the increase of χ_{min} with fluence. As the energy E used in their experiment (2 MeV) is different from ours (0.3 MeV), the corresponding fluence is scaled with $1/E$ [16]. Therefore, the same damage was produced in both experiments and it can be seen from table 2 that the decrease in T_c is accompanied by a decrease in $\psi_{1/2}$ and an increase in χ_{min}.

5. Discussion

The most intriguing question for a superconductor with the A15 structure such as V_3Si is what kind of damage causes the large depression of T_c after irradiation. At high He-fluences T_c was found to saturate at about 2.5 K for V_3Si and similar T_c-values have been observed for highly disordered V_3Si thin films deposited at room temperature [4]. This damage is similar to the heavy ion damage forming amorphous zones.

The lower saturation level of T_c has been observed in the region of light ion damage (film thickness about 2000 Å, He-ion energy 2 MeV). In this region

the density of amorphous zones is small and no direct backscattering is observed. If we assume that the amount of the dechanneling component is due to the existence of extended defects, a concentration of about $10^{17}/cm^3$ has been estimated. In Nb_3Sn irradiated with neutrons extended defects with an average size of 40 Å diameter have been observed [7]. Assuming the same average diameter a maximum fraction of disordered volume is then calculated to be about 0.017.

In order to describe the measured data [4] using eq. 4 for the T_c-decrease with increasing fluence shown as a solid line in fig. 6, the following values were used:
$N_s V_s$ and $N_n V_n$ have been obtained from the BCS–formula using $T_c = 16.5$ and $T_c = 2.5$, respectively and $\theta_b = 450$ K. At the He-fluence of $3.3 \times 10^{17}/cm^2$ where T_c reaches the lower saturation level, F was assumed to be 0.6. A close fit to the experiment is reached if the ratio N_s/N_n is assumed to be equal to 5. Although the measured data are described rather well, there are two main objections:

i) the large decrease of N_s should be accompanied by simultaneous yet somewhat smaller increase in V_s, in contradiction to the findings in [8].

ii) An upper limit in the number of extended defects as estimated from dechanneling yield for a fluence corresponding to 3.3×10^{17} He/cm^2 of 2 MeV is $5 \times 10^{17}/cm^3$ resulting in $F = 0.017$ which is small compared to the value of $F = 0.6$ used as a fit parameter at this fluence.

The most probable explanation for the observed narrowing of the critical angle and the increase of the minimum yield as function of depth (identical to an increase of the dechanneling component) is the assumption of small displacements of the V atoms from the row. The existence of such damage structures (a "zig-zag" arrangement) has been suggested previously [8] as a possibility for the transition metal atoms in the chain to release compression. As a severe consequence, the symmetry of the system is disturbed [25]. Weger [26] showed that the matrix elements of interchain coupling are large, however because of symmetry considerations their influence on the sharp peaks of the electron state density cancels. If the symmetry is abolished this coupling will destroy the sharp peaks in the density of electronic states and thus depress T_c.

Acknowledgements

The author would like to thank M. Kraatz for implantation, Dr. J. Geerk for sample annealing and Dr. E.L. Haase for reading the manuscript.

References

[1] A.R. Sweedler, D.G. Schweitzee and G.W. Webb, Phys. Rev. Lett. 33 (1974) 168.
[2] O. Meyer, H. Mann and E. Phrilingos, in Application of Ion Beams to Metals, S.T. Picraux, E.P. EerNisse and F.L. Vook, ed. (Plenum Press, N.Y. 1974).
[3] B. Besslein, G. Ischenko, S. Klaumünzer, P. Mueller, H. Neumueller, K. Schmelz and H. Adrian, Phys. Lett. 53A (1975) 49.
[4] K.M. Poate, R.C. Dynes, L.R. Testardi and R.H. Hammond, in: Superconductivity in d- and f-Band Metals, D.H. Douglass, ed (Plenum Press, N.Y. 1976).
[5] A.R. Sweedler and D.E. Cox, Phys. Rev. B12 (1975) 147.
[6] J. Appel, Phys. Rev. B13 (1976) 3203.
[7] C.S. Pande, BNL Report 22248.
[8] C.M. Yarma and R.C. Dynes (see ref. 4).
[9] J.W. Mayer, L. Eriksson and J.A. Davies, in: Ion Implantation in Semiconductors (Academic Press, N.Y. 1970).
[10] K.L. Merkle, P.P. Pronko, D.S. Gemmell, R.C. Mikkelson and J.R. Wrobel, Phys. Rev. B8 (1973) 1002.
[11] M. Gettings, O. Meyer and G. Linker, Rad. Eff. 21 (1974) 51.
[12] Y. Quéré, Rad. Eff. 28 (1976) 253.
[13] P. Baeri, S.K. Campisano, G. Foti, E. Rimini and J.A. Davies, Appl. Phys. Lett. 26 (1975) 424.
[14] V_3Si were obtained from B. Seeber, Universität München, Forschungslaboratorium für Festkörperchemie, Leiter: Dr. J.J. Nickl.
[15] Ion Beam Surface Layer Analysis, J.W. Mayer, J.F. Ziegler, Thin Solid Films, ed. 19 (1973) 423.
[16] P. Sigmund, Rev. Roumaine Physique 17 (1973).
[17] J.H. Barrett, Phys. Rev. B3 (1971) 1527.
[18] J. Lindhard, Kgl. Danske Videnskab. Selskab. Mat.-Fys. Medd. 34 no. 14 (1965).
[19] P.G. DeGennes, Rev. Mod. Phys. 36 (1964) 225.
[20] P.B. Bansal and A.J. Ardell, Metallography 5 (1972) 97.
[21] J.L. Staundenmann, P. Coppens and J. Mueller, Solid State Comm. 19 (1976) 29.
[22] J.A. Davies, G. Foti, L.M. Howe, J.B. Mitchell and K.B. Winterbon, Phys. Rev. Lett. 34 (1975) 1441.
[23] R. Kaufmann and E.L. Haase, Private communication.
[24] A detailed evaluation of the channeling results in V_3Si prior to implantation will be published elsewhere.
[25] H. Rietschel, private communication.
[26] M. Weger, Solid State Physics 28 (1973) 145.
[27] O. Meyer and B. Seeber, Solid State Comm. 22 (1977) 603.

Discussion

C. Pande: Dr. Meyer's otherwise excellent paper makes some unwarranted criticism of the model of T_c degradation in A15's on irradiation presented by me in this meeting. This criticism is based on an incorrect interpretation of his data. In particular:

1) The size of the disordered regions of 40 Å for 300 kV α-particles is an order of magnitude too large. [See for example, M.W. Thompson Defects and Radiation Damage in Metals, Cambridge University Press. Cambridge, England (1969)]. The value of 35 Å obtained by me experimentally is for high energy ($E > 1$ MeV) neutrons and *not* α-particles.

2) The volume fraction F_v is defined in my model (see this conference proceedings) as $F_v = (1 - e^{-k\phi t})$ where ϕt is the fluence, and represent the fraction of the atoms disturbed. My model is valid provided these disturbed atoms form inhomogeneous regions where the Cooper pair correlation amplitude has a value different from that of the undisturbed regions. Dr. Meyer mistakenly identifies this F_v, with the volume fraction of his sample having some kind of strain.

3) The calculation of T_c on the proximity effect model using the *corrent* F_v then should follow the method given by Silvert (Physical Review 1975)

by Silvert (Physical Review 1975) and Pande (Solid State Communication 1977).

O. Meyer: An increase in the minimum yield $\chi_{min}(t)$ as a function of depth (or in the dechannelling component) was found in Au-single crystals after irradiation with 2 MeV He and was attributed to defect clusters or disordered regions (extended defects) with an average cluster diameter of 38 Å (TEM-results) [10]. The maximum recoil energy transferred to Si atoms by 300 keV α-particles is 130 keV, large compared to the average energy of 60 keV for those cascades that produce visible clusters [10]. Assuming the existence of such defect clusters for the irradiated V_3Si together with the observed increase of $\chi_{min}(t)$ in the fluence region where the T_c-depression is saturated, the estimated disordered volume fraction is 0.017. Strain fields from clusters are included in the dechanneling cross section used for the calculation, that means that the value of $F_v = 0.017$ is an upper limit. This value however is far too small in order to explain the T_c-depression by the proximity effect. The existence of such extended defects would also be in contradiction to my discussion on the heavy ion defects, where substantial diffusional effects have not been observed.

Both the increase in $\chi_{min}(t)$ and the narrowing of $\psi_{1/2}$ can be explained by the existence of a small displacement with gaussian distribution of nearly all V-atoms from their lattice site [27]. This defect, we believe, is responsible for the large T_c-depressions observed for A15 material after He irradiation [4].

So the question remains, what kind of defect is responsible to explain the observed T_c-depression in n-irradiated A15 material. To solve this question, channeling measurements on n-irradiated V_3Si single crystals should be performed.

B.R. Appleton: Since it may be difficult for those outside the channeling field to assess the results presented, I would just like to comment as one who is somewhat familiar with the field. The measured "signal" from these results is certainly consistent with a static displacement of the lattice atoms. Whether the displacement is 0.1 Å or 0.2 Å is a matter of interpretation of the channeling model, but there is little doubt that the effect is real and that Otto's interpretation is a corrent one. The origin of this displacement (defect) cannot be made clear from the present measurements but might, in fact, be possible to reconcile from more detailed channeling measurements. The displacement could be some stabilized defect, lattice strain etc. but the channeling measurements reported certainly reflect lattice atom displacements.

O. Meyer: I agree that the chaneling model is still not good enough to give very precise absolute numbers of $\langle u \rangle$. However as we have performed a relative measurement before and after irradiation we may base our results on the X-ray data [21]. Assuming static displacements with gaussian distribution and subtracting the square of the rms one-dimensional thermal vibrational amplitude we obtain the values for the one-dimensional rms static displacements to be 0.06 Å perpendicular to the [100]- and 0.09 perpendicular to the [110] direction.

H. Freyhardt: How do the measured displacements $\langle u \rangle$ compare to the T_c-depression; are both saturating for the same fluence?

O. Meyer: Table 2 indicates that the decrease of $\psi_{1/2}$ and the increase of χ_{min} correlates with the T_c-decrease as measured by Poate et al. [4] using two 2 MeV He-ions. The scaling factor $1/E$ (E = incident He ion energy) was used to determine the corresponding dose for 300 keV He ions. In the meantime T_c versus fluence curves have been measured on thin V_3Si films using 300 keV He ions (the films have kindly been given to us by L.R. Testardi). The results show, that the corresponding fluence for 300 keV He is about a factor of 10 smaller than that for 2 MeV He. Therefore, the corresponding fluences for 300 keV He as given in table 2 should be multiplied by a factor of 1.5, with the result that the correlation is shifted to the steep part of the T_c depression curve.

Journal of Nuclear Materials 72 (1978) 275–281

INFLUENCE OF ION BOMBARDMENT ON THE SUPERCONDUCTING TRANSITION TEMPERATURE OF EVAPORATED VANADIUM LAYERS

G. LINKER

Kernforschungszentrum Karlsruhe, Institut für Angewandte Kernphysik, 7500 Karlsruhe, Postfach 3640, Fed. Rep. Germany

The influence of ion irradiation and implantation on the superconducting transition temperature T_c of evaporated vanadium layers has been investigated as a function of ion species and layer purity. Irradiations of pure layers with Ne^+ ions and fluences of typically 10^{16} ions/cm^2 lead to small T_c decreases ($\Delta T_c \sim 0.1-0.2$ K). In oxygen contaminated layers however appreciable changes of T_c ($\Delta T_c \sim 2-3$ K) are observed depending on oxygen content and ion fluence. Similarly, the direct implantation of chemically active impurities (N^+, O^+) leads to drastic changes of T_c. Here T_c decreases as a function of nitrogen concentration down to the detection limit of 1.2 K. From these results it is concluded that the T_c changes are due to impurity stabilized disorder. Energy dependent chanelling analysis of nitrogen and neon implanted V and Mo single crystals has been performed to obtain additional information on the nature of this disorder.

L'influence de l'irradiation et de l'implantation ionique sur la température de transition supraconductrice T_c de couches de vanadium évaporées a été étudiée en fonction des espèces d'ions et de la pureté de la couche. Des irradiations de couches pures par des ions Ne^+ sous des fluences de 10^{16} ions cm^{-2} conduisent à de faibles diminutions de T_c($\Delta T_c \sim 0{,}1-0{,}2$ K). Dans des couches contaminées par de l'oxygène cependant, des variations appréciables de T_c($\Delta T_c \sim 2-3$ K) sont observées qui dépendent de la teneur en oxygène et de la fluence ionique. De même, l'implantation directe d'impuretés chimiquement actives (N^+, O^+) conduit à des variations importantes de T_c. Ici T_c diminue en fonction de la concentration en azote jusqu'à la limite de détection de 1, 2 K. De ces résultats on conclut que les variations de T_c sont dues au désordre stabilisé par les impuretés. L'analyse par canalisation en fonction de l'énergie de monocristaux de V et Mo implantés en azote et néon a été effectuée afin d'obtenir une information complémentaire sur la nature de ce désordre.

Es wurde der Einfluss von Ionenbestrahlung und Implantation auf die Übergangstemperatur zur Supraleitung T_c in aufgedampften Vanadium-Schichten als Funktion der Ionensorte und der Schichtreinheit untersucht. Die Bestrahlung reiner Schichten mit Ne^+-Ionen und Fluenzen von typisch 10^{16} Ionen/cm^2 führte zu geringen T_c-Absenkungen ($\Delta T_c \approx 0{,}1-0{,}2$ K). In sauerstoffverunreinigten Schichten wurden jedoch erhebliche T_c-Änderungen ($\Delta T_c \approx 2-3$ K), die vom Sauerstoffgehalt und der Ionenfluenz abhingen, beobachtet. Auf ähnliche Weise führte die direkte Implantation chemisch aktiver Verunreinigungen (N^+, O^+) zu drastischen T_c-Änderungen. Dabei wurde T_c als Funktion der Stockstoffkonzentration bis zur Nachweisgrenze von 1,2 K abgesenkt. Aufgrund dieser Ergebnisse wird geschlossen, dass die T_c-Änderungen durch eine verunreinigungsstabilisierte Störung der Schichten bewirkt werden. Es wurden energieabhängige Channellingmessungen an stickstoff- und neonimplantierten V- und Mo-Einkristallen durchgeführt, um zusätzliche Informationen über die Art dieser Störung zu erhalten.

1. Introduction

Disorder introduced in superconductors may lead to considerable changes of the superconducting transition temperature T_c. A high degree of disorder in metal films is introduced by vapour deposition onto cryogenic substrates and substantial variations of T_c have been observed in several transition metal layers [1,2]. The important role of impurities in stabilizing disordered phases in quench condensed Mo and Nb layers has been described recently by Schroeder et al. and the disordered structure ascertained in terms of a DRPHS model [3].

Ion irradiation also leads to disorder in materials due to energy deposited in nuclear collision along the paths of the bombarding particles. The effects of irradiation on the superconducting properties have been mainly studied with neutrons and light ions and striking changes were reported for the critical current density. However, small effects were observed for T_c in tran-

sition metal elements. After heavy ion bombardment however we have found strong T_c depressions in evaporated V, Nb and Ta layers in earlier studies [4,5]. These depressions were attributed to radiation damage deteriorating the bcc structure of the layers. The influence of impurities on the results could not be excluded in these investigations, since it was not explicitly studied. The importance of impurities present in a layer on changes of T_c after ion bombardment have been demonstrated in experiments with low-temperature ion implanted molybdenum layers [6]. Here an increase of T_c with noble gas ion bombardment has been observed in oxygen contaminated layers. The increase was dependent on ion fluence and oxygen concentration with a lower limit of about 1 at.%. Also the direct implantation of chemically active impurities into pure molybdenum layers has been found to increase T_c and has been studied in detail together with structural transformations after nitrogen implantations [7]. A maximum T_c value of 9.2 K for 23 at.% nitrogen implanted at low temperatures accompanied by a strongly distorted bcc structure of Mo were the main results of this study. The stabilization of the disordered phase observed in these experiments has been ascribed to the interaction of the chemically active impurity atoms with the distorted host lattice as no such effects were observed either with bombardment or implantation of noble gas ions.

In this present contribution results from a similar study performed with vanadium layers will be reported. In an extension of our previous work on group Vb transition metal elements, in these irradiation experiments the influence has been investigated on the critical temperature T_c of activated impurities present in a layer and of implanted impurity atoms. Together with the layer experiments, energy dependent channelling studies on Ne or N implanted vanadium and molybdenum single crystals have been performed in order to obtain information on the different structure of the defects produced either with neon or nitrogen.

2. Experimental

The V layers were deposited onto quartz, sapphire and carbon substrates by electron beam evaporation. The background pressure in the evaporation chamber prior to evaporation was typically 2×10^{-9} torr and rose to 5×10^{-9} torr at evaporation rates of 10 Å/s and to 1×10^{-7} torr at the maximum rate of 160 Å/s. Substrates were baked prior to evaporation in situ; deposition then was performed either on substrates kept at room temperature or heated to 560–800°C. To introduce oxygen into the layers the oxygen partial pressure during evaporation was varied in the range between 5×10^{-8} and 5×10^{-6} torr.

Layer thickness, purity and homogeneity, the oxygen content and distribution have been analyzed by Rutherford backscattering [8] of 2 MeV $^4He^+$ ions. Layers deposited onto the carbon substrates were used for this analysis thus allowing an oxygen concentration determination down to about 0.2 at.%.

Implantations and irradiations were performed at room temperature with Ne^+ or N^+ ions, respectively. An energy of 320 keV has been used for the layer irradiation with Ne^+ such that the ions penetrated the layers and came to rest in the substrates. The profile of the energy deposited in nuclear collisions along the paths of particles creating damage in a layer is shown in fig. 1. A straight path of the particles (range = projected range) through a layer of 2000 Å thickness has been assumed in this profile calculation described in detail elsewhere [5].

In order to obtain a constant concentration of N or Ne in the implantation experiments over the total layer thickness several different energies were used. The fluences for each energy were determined by the calculation of added depth distributions using values of projected range and straggling in projected range tabulated by Johnson and Gibbons [9]. An example

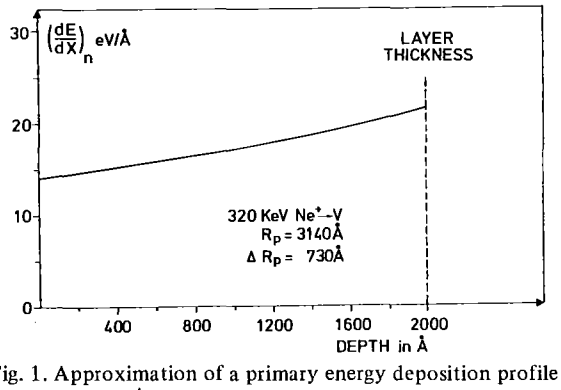

Fig. 1. Approximation of a primary energy deposition profile for 320-keV Ne^+ ions in a 2000 Å thick vanadium layer. $dE/dx|_n$ represents the nuclear stopping power.

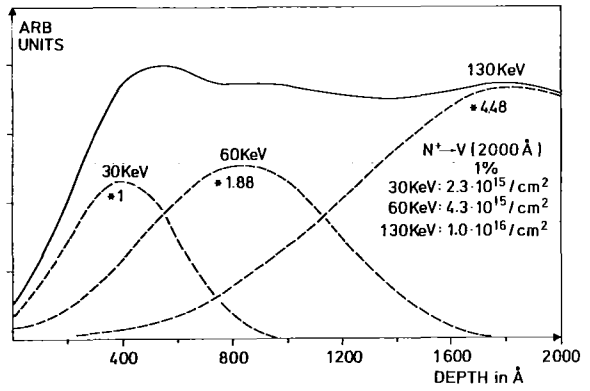

Fig. 2. Calculated implantation profile for nitrogen in vanadium with three different energies. Fluence values for a nitrogen concentration of 1% are indicated in the figure. Fluences for the higher energies are to be multiplied by the calculated values (indicated at the single profiles) if the fluence for the lowest energy is normalized to 1.

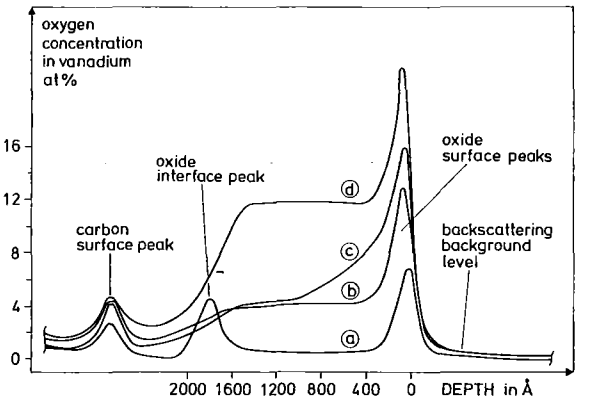

Fig. 3. Sections of 2 MeV, $^4He^+$ backscattering spectra of V layers on C substrates showing different oxygen distribution profiles. (a) layer with a low homogeneous oxygen content exhibiting an oxide peak at the layer–substrate interface, (b) and (d) layers with medium and high oxygen content with reasonable homogeneity (c) sample with inhomogeneous oxygen distribution.

of such a calculated profile for nitrogen implanted in a 2000 Å thick vanadium layer together with the profiles for the single energies is shown in fig. 2. The calculation procedure is described in detail elsewhere [10]. The superconducting transition temperature, defined as the midpoints of the transition curves, was determined resistively using a standard four-probe arrangement. The lowest temperature attainable in our cryostat was about 1.2 K.

3. Results and discussion

3.1. Analysis of "as-evaporated" layers

The as-evaporated vanadium layers had thicknesses of 1500 to 2500 Å and did not depend on the different substrate materials. Oxygen concentration and distribution determined from layers deposited on carbon substrates were assumed to be the same as in layers on quartz or sapphire substrates. All the layers revealed a pronounced oxide peak on the layer surfaces and sometimes an oxygen peak was observed at the layer–substrate interface. In addition to the surface oxide peak, some layers showed a diffusion tail into the layer thus indicating a rather inhomogeneous oxygen distribution and complicating the interpretation of the irradiation experiments. Typical oxygen distribution profiles deduced from backscattering spectra are shown in fig. 3. Layers with the lowest oxygen content were produced at elevated substrate temperatures where oxygen concentrations from 1.5 at.% to "not detectable" (~0.2 at.%) were found. However, layers deposited at similar evaporation conditions onto substrates kept at room temperature revealed higher oxygen contents ranging from 1.5 to about 4 at.%. No significant differences in impurity concentration were found for different optimum evaporation conditions, i.e. "good" vacuum ($\sim 5 \times 10^{-9}$ torr) and low rate (~10 Å/s) or "bad" vacuum ($\sim 1 \times 10^{-7}$ torr) and high deposition rate (~160 Å/sec), but high rates appeared to result in a more homogeneous impurity distribution. However, this point has not been studied in detail. Layers prepared under oxygen atmosphere had oxygen concentration in the range of 4 to 40 at.%.

The transition temperatures T_c of the as-evaporated layers were in the range of 4.9–5.25 K while the transition widths had values of about 0.05 K. These values did not depend on oxygen concentration in the range of a few at.% thus indicating that oxygen must have been incorporated in the layers in the form of oxide precipitates, as oxygen dissolved in V would drastically lower T_c in this concentration range [11]. Similarly, the residual resistivity ratio values r (defined as the ratio of resistivities at room temperature and just before the transition into the superconducting state)

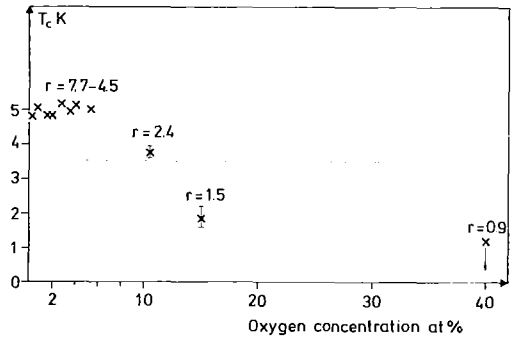

Fig. 4. T_c and residual resistivity values r in evaporated vanadium layers as a function of oxygen concentration.

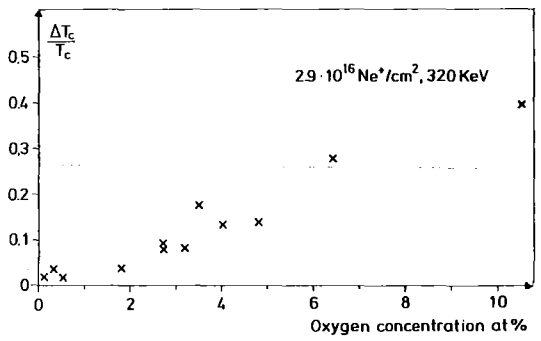

Fig. 5. Relative T_c depressions $\Delta T_c/T_c$ in layers irradiated with 2.9×10^{16} (320-keV Ne^+)/cm^2, as a function of oxygen concentration.

showed no close correlation with oxygen content and values for r of 4.5 to 6 were found in layers with a few at.% oxygen. The best values were found in layers with a small oxygen content (<1%) and the maximum r of 11 was measured in layers where no oxygen could be detected with the backscattering technique. Beyond an oxygen content of about 5 at.% T_c decreased with oxygen concentration accompanied by a decrease of r and an increase in the transition width. This behavior is illustrated in fig. 4. X-ray diffraction patterns from the layers with high oxygen content (10.5 and 15 at.%) showed the strongest vanadium bcc lines, but the lines were considerably broadened as compared to lines from a pure sample. This broadening increased with oxygen content. In addition, a line shift to lower angles was observed from which a lattice parameter increase of about 0.5% has been estimated. The layer with 40 at.% oxygen revealed an "amorphous-like" structure.

3.2. Neon irradiation

Two different experiments were performed with neon ion irradiations. First a constant fluence of neon ions has been used and layers with varying oxygen content were irradiated. Secondly, layers with the same oxygen content were irradiated with different Ne^+ fluences. In both experiments an incident energy of 320 keV has been used, such that most particles penetrated the vanadium layers (projected range in vanadium >3000 Å) and were deposited in the substrates. A fluence of 2.9×10^{16} Ne^+/cm^2 was used in the first experiment corresponding to approximately 20 dpa (displacements per atom) as estimated from the energy deposition profiles. A decrease of the transition temperature has been observed in both experiments. The results from the first one are shown in fig. 5 where the relative decrease ($\Delta T_c/T_c$) of T_c is plotted as a function of oxygen concentration. For the vanadium layers with the lowest oxygen content small depressions in the range of 0.1–0.2 K were observed. With increasing oxygen content more drastic effects occur with relative changes up to 0.4. Together with T_c, the residual resistivity ratio r also decreases as a function of oxygen content and an increase of the transition width is observed.

Similar effects were found in the second experiment by irradiating layers with constant oxygen content with fluences in the range of 9.2×10^{15} to 2.9×10^{17} Ne^+/cm^2. The results for a typical layer are shown in fig. 6. Here T_c decreases as a function of fluence and simultaneously r decreases and the transition width broadens.

There were some difficulties in obtaining quantitatively reproducible results due to inhomogeneous oxygen distribution in the layers, possible variation of the grain size in layers prepared under different deposition conditions, and some general difficulties in irradiation experiments with thin films (e.g. recoil implantation from surface oxide, sputtering effects at high fluences, resistive T_c measurements). Despite these difficulties, these data demonstrate the important role of impurities on the T_c reductions in vanadium layers. Samples with very low oxygen content show decreases similar to those observed in niobium samples with high integrated fast neutron fluences [12]. However,

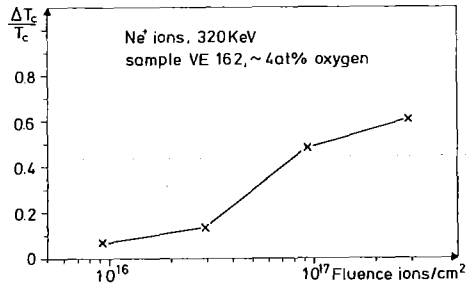

Fig. 6. Relative T_c depressions in a layer with 4 at.% oxygen as a function of ion fluence (Ne^+, 320 keV).

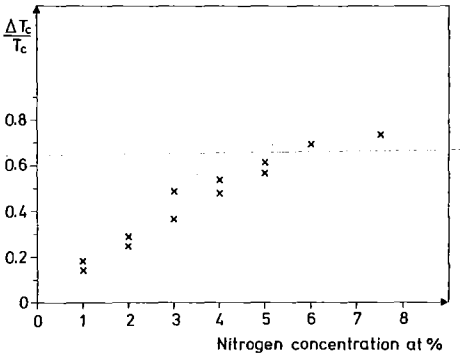

Fig. 7. Relative T_c decreases in vanadium layers implanted with nitrogen as a function of nitrogen concentration.

with increasing oxygen content T_c decreases drastically. It is thought that in oxygen contaminated samples, either an increase in oxygen content or an increase in fluence, in principle cause the same effect, namely raise the probability of oxygen atoms being moved from an inactive position (such as oxygen present in oxide precipitates) to an "active" position (such as interacting with displaced lattice atoms). With this idea T_c decreases necessarily should saturate when all impurity atoms would be activated. However, a saturation value could not be established as in some samples (especially in relatively thin layers even with low oxygen concentrations ~0.5%) T_c reductions down to the detection limit (1.2 K) occured. This effect for very high fluences was observed already in our earlier work on group Vb transition metals and was assigned to macroscopic distortions of the layers as detected by the backscattering technique [5].

3.3. Nitrogen, oxygen and neon implantations

Oxygen dissolved in group Vb elements is known to reduce T_c by about 1 K/at.% [11]. Therefore, the question arose whether in the irradiation experiments the activated position of oxygen may be dissolved oxygen thus reducing T_c. For clarification nitrogen and neon have been homogeneously implanted into vanadium layers with the least oxygen content. Here also T_c reductions have been observed, the effect being much more pronounced for nitrogen. The relative T_c changes as a function of nitrogen concentration are illustrated in fig. 7 and an almost linear relationship between $\Delta T_c/T_c$ and nitrogen concentration is observed down to the T_c detection limit. The T_c reductions, similar to the irradiation experiments, are accompanied by decreases of the residual resistivity ratio. Neon implantations also lead to T_c reductions, however the effect is much smaller than for nitrogen. For example, 5 at.% implantations into similar layers yield relative reductions of 0.61 and 0.14 for nitrogen and neon, respectively, although more energy is deposited in nuclear collisions by the neon ions.

In addition to the neon and nitrogen implantations, a comparison of two identical implantations with nitrogen and oxygen ions (3 at.% profiles) were performed. Oxygen and nitrogen have quite different solubility levels in vanadium. Relying on the data compiled by Hansen [13], the solubility of N in V is very small and lattice parameter measurements indicated a value of about 0.66 at.%. For O in V most reliable measurements (see ref. 13) quote a value of 3.2 at.%. Though the effect on T_c of nitrogen dissolved in V is not known, it may be assumed to be small as concluded from results of nitrogen in Nb [11]. In the implantation experiment relative T_c depressions of 0.38 and 0.41 for nitrogen and oxygen respectively, were found, which agree within the error limits for these experiments and also the reduction of the residual resistivity ratio and the increase of the transition widths observed in the oxygen implanted samples were in close agreement with those of the nitrogen implanted ones. This comparison shows that oxygen and nitrogen, both having high electronegativity values, cause the same effect in contrast to neon.

Thus, it is also concluded that in the irradiation experiments the T_c depression in oxygen contaminated samples is not due to oxygen being dissolved in the irradiation procedure (alloying effect) but that, similar

to the experiments of implantation into molybdenum layers [7], disorder introduced into the vanadium matrix is the main reason for this effect. This disorder generated during irradiation must be stabilized by the chemically active either implanted (nitrogen) or activated impurity (oxygen) atoms which are interacting with the displaced lattice atoms. It is at present not clear whether inert gas ions (neon) may have a disorder stabilizing effect. It is thought that the T_c reductions observed with Ne implantations are due to secondary effects like activation of oxygen still present in our best layers or recoil implantations from surface oxide or substrate, though these last processes are not very likely. Strong variations of T_c together with sizeable lattice expansions have been reported, however, by Schmidt et al. [14] in transition metals deposited with noble gases. Channelling experiments and preliminary X-ray investigations have been performed to obtain some information on the nature of the defects created in our irradiation and implantation experiments.

3.4. Channelling experiments

Channelling experiments were performed on Ne- or N-implanted V and Mo single crystals. Energy dependent analyses have been performed following the suggestions of Quéré [15]. This should allow a determination of at least the leading contribution of a certain kind of defects from the energy dependence of the dechannelling cross section. Results from this dechannelling analysis will be reported in greater detail elsewhere [16]. Briefly, the analysis of vanadium crystals bombarded with 2.9×10^{16} (320-keV Ne^+)/cm^2, simulating an irradiation through a 2000 Å thick layer, shows that extended defects like voids or dislocations are produced throughout this depth. Implantations of nitrogen into a near surface layer, however, revealed a peak in the backscattering spectra indicating the presence of locally displaced host lattice atoms probably fixed to their new position by interaction with the implanted impurities. This peak smaller than for nitrogen is also observed for neon in contrast to channelling experiments in Mo. Pure Mo layers in accordance with this result did not show T_c increases with Ne implantations. Thus it can not be excluded that the small T_c decreases in V layers by neon implantation are the result of disorder stabilized by the neon itself.

3.5. X-ray analysis

Preliminary X-ray analysis has been performed on samples where the lowest T_c values were observed after implantation or irradiation utilizing a commercial thin film Seemann–Bohlin film camera. All bombarded samples revealed the vanadium bcc structure, however a line broadening and an increase in lattice parameter have been observed in irradiated samples containing oxygen or in pure layers implanted with nitrogen. The increase in lattice parameter was higher for the nitrogen implanted samples (about 1%) than for the irradiated samples (about 0.5%) and seemed to depend on nitrogen concentration. In contrast to these results no change in the lattice parameter has been found in the neon implanted sample (5 at.%) within the accuracy limits of this analysis.

4. Conclusions

The aim of this investigation was to study the influence of impurities on the depression of the superconducting transition temperature T_c in heavy-ion irradiated vanadium layers. Despite some scatter in the experimental results it has been found that chemically active impurities play an important role in the T_c decreases. These impurities can be either implanted into the layers or activated, i.e. moved from oxide precipitates into the vanadium grains by recoil implantation during irradiation with noble gas ions. Similar T_c depressions have been obtained with oxygen and nitrogen implantations. Thus, it is unlikely that the observed effects are caused by alloying, but rather it is assumed that the T_c depressions are due to disorder in the host lattice itself. The structure of this disorder is not completely clear. Channelling experiments, however, suggest that locally displaced lattice atoms are present in the irradiated samples. These atoms must be stabilized in their new positions by interaction with either implanted or activated impurities. Here chemically active impurities were found to act much more effectively than neon whose role could not be clearly estimated.

A saturation value for the T_c depressions could not be established since in the irradiation and implantation experiments almost linear decreases in T_c have been observed as a function of fluence or concentra-

tion down to the detection limit. Since the X-ray analysis of the samples bombarded with high fluences still showed the vanadium bcc structure it is thought that more disorder can be introduced into the samples either with higher impurity concentrations or with ion bombardment at low temperatures. This agrees with the observations in implantation experiments of Mo layers where a quasi amorphous phase has been found at about 23 at.% nitrogen implanted at liquid He temperature. However, it is not known at present whether the same impurity concentration is necessary in V and Mo to stabilize an amorphous phase with T_c at the saturation level. An open problem is also the question of how the T_c in the layers is affected qualitatively as a function of nitrogen concentration. It may be that small distorted regions (e.g. impurity defect clusters) are produced with a low T_c (saturation) and the number of these regions grow with nitrogen concentration and reduce the T_c of the unaffected V by the proximity effect. On the other hand, a distorted homogeneous phase is possible throughout a layer with the degree of disorder growing with impurity concentration and the T_c depending on the degree of disorder. Further experiments with high impurity concentrations and implantation at low temperatures are planned to explore whether (similar to Mo) amorphization occurs in group Vb transition elements in irradiation experiments.

Acknowledgements

The author would like to thank R. Smithey for the V layer evaporations, M. Kraatz for performing the implantations, O. Meyer and P. Ziemann for many helpful discussions.

References

[1] J.E. Crow, M. Strongin, R.S. Thompson, O.F. Kammerer, Phys. Lett. 30A (1969) 161.
[2] M.M. Collver, R.H. Hammond, Phys. Rev. Lett. 30 (1973) 92.
[3] B. Schroeder, W.L. Johnson, C.C. Tsuei, P. Chandhari, J.F. Graczyk, AIP Conf. Proc. (USA) 31 (1976) 353.
[4] O. Meyer, H. Mann, E. Phrilingos, in: Application of Ion Beams to Metals, S.T. Picraux, E.P. EerNisse, F.L. Vook, eds. (Plenum Press, New York, 1974) p. 15.
[5] G. Linker, O. Meyer, in: Ion Implantation in Semiconductors, S. Namba ed. (Plenum Press, New York, 1975) p. 309.
[6] O. Meyer, Inst. Phys. Conf. Ser. No. 28 (1976) 168.
[7] G. Linker, O. Meyer, Sol. State Comm. 20 (1976) 695.
[8] J.W. Mayer, L. Eriksson, J.A. Davies, in: Ion Implantation in Semiconductors (Academic Press, New York and London, 1970) p. 136.
[9] W.S. Johnson, J.F. Gibbons, Projected Range Statistics in Semiconductors, (Stanford, Calif. 1970).
[10] G. Linker, Progress Report of the Teilinstitut Nukleare Festkörperphysik, G. Heger ed. (1976) p. 86.
[11] W. DeSorbo, Phys. Rev. 132 (1969) 107.
[12] R.H. Kernohan, S.T. Sekula, J. Appl. Phys. 38 (1967) 4904.
[13] M. Hansen, The Constitution of Binary Alloys (McGraw Hill, New York, 1958).
[14] P.A. Schmidt, R.N. Castellano, H. Barz, A.S. Cooper, E.G. Spencer, J. Appl. Phys. 44 (1973) 1835.
[15] Y. Quéré, Rad. Eff. 28 (1976) 253.
[16] G. Linker, III Int. Conf. on Ion Beam Analysis, Washington, D.C. June 1977.

NUCLEAR INSTRUMENTS AND METHODS 149 (1978) 365-369 ; © NORTH-HOLLAND PUBLISHING CO.

CHANNELING ANALYSIS OF RADIATION DISORDER IN ION IMPLANTED VANADIUM AND MOLYBDENUM SINGLE CRYSTALS

G. LINKER

Institut für Angewandte Kernphysik, Kernforschungszentrum Karlsruhe, 7500 Karlsruhe, Postfach 3640, W. Germany

Energy dependent channeling and backscattering analysis with $^4He^+$ ions in the energy range 1.0–2.8 MeV has been performed on V and Mo single crystals implanted either with Ne^+ or $N^+(C^+)$ ions ($\sim 5\times 10^{16}$ ions/cm^2). The spectra of the implanted samples revealed an appreciable amount of dechanneling but only a small energy dependence of the dechanneling yield was observed. However, characteristic differences of the dechanneling profiles were detected in the Ne^+ and N^+ implanted crystals. The Ne^+ bombarded samples showed an almost linear increase of the dechanneling yield with depth but showed no change of the shape of the spectra as a function of analyzing beam energy. In contrast, the N^+ implantations revealed a peak in the spectra at the range of the implanted impurities as the beam energy was increased. These observations indicate that different types of defects are generated with implantations of Ne^+ and N^+ ions. The results are discussed together with changes of the superconducting transition temperature in ion implanted and irradiated V and Mo layers.

1. Introduction

Channeling effect and backscattering measurements with energetic light ions have been widely employed for defect analysis in ion implanted semiconductors[1]). Here in the aligned spectra a well resolved disorder peak is usually observed at the range of the implanted ions originating from direct backscattering of the probing particles from displaced lattice atoms. Aligned backscattering spectra from ion bombarded metals, however, generally reveal a monotonous increase of the dechanneling yield and show no damage peak[2–4]) due to the different defect structures in these materials. This behaviour complicates the disorder analysis in metals with the channeling technique; successful approaches have however been undertaken by correlating dechanneling cross-sections with damage observation from transmission electron microscopy (TEM)[5]). The simultaneous use of the channeling-backscattering technique and TEM is at present a promising procedure to correlate dechanneling observations with damage configurations in metals. In addition, by dechanneling analysis itself, different types of defects may be separated when energy dependent measurements are performed as has been suggested by Quéré[6]). This method relies on the different energy dependences of dechanneling cross-sections. Dechanneling yields depending on energy as $E^{\frac{1}{2}}$ would indicate dislocations, E^0-dependence, e.g. stacking faults or gas bubbles, and E^{-1}-dependence, randomly distributed atoms[7]). Defect analysis of ion implanted Al single crystals utilizing these energy dependences of the dechanneling has already been performed, e.g. by Rimini et al.[8]).

In this contribution, results from energy dependent analysis of neon and nitrogen (or carbon) implanted vanadium and molybdenum single crystals are reported. The problem stems from ion implantation and irradiation experiments of V and Mo superconducting layers where changes of the superconducting transition temperature T_c have been observed; these changes had been observed to depend on layer purity and the nature of the implanted ion. In Mo, e.g. the implantation of chemically active ions (N^+, C^+) led to T_c increases, while Ne^+ caused no effect in pure layers but increased T_c in oxygen contaminated layers and low temperature irradiations. Similar effects with lowering of T_c were observed in V layers. These results, which are published in greater detail elsewhere[9–11]), indicated that the T_c-changes are correlated with radiation induced, impurity stabilized types of defects. Therefore parallel experiments with implanted V and Mo single crystals have been performed to obtain some information on the nature of these defects.

2. Experimental

Vanadium single crystals were implanted with Ne^+ and N^+ ions at 320 keV and 50 keV to fluences of 2.9×10^{16} Ne^+/cm^2 and 5.1×10^{16} N^+/cm^2, respectively. For molybdenum Ne^+ and C^+ ions were used with energies of 50 keV and 100 keV and fluences of 2.7×10^{16} C^+/cm^2 and 5.5×10^{16} Ne^+/cm^2, respec-

tively. All implantations were performed at room temperature. A vanadium layer of about 600 Å thickness was evaporated on top of a vanadium single crystal to test the dechanneling behaviour of a highly disordered region.

Channeling and backscattering analysis was performed with $^4He^+$ ions at energies of 1.0, 1.5, 2.0 and 2.8 MeV. The samples were aligned along the [100] direction and backscattered particles were detected at 165° and analyzed with standard electronics. Backscattering spectra from random and aligned samples were taken before and after implantation, samples were rotated around an axis well off the channeling direction for detection of the random spectra.

3. Results

3.1. Evaporated vanadium layer

The atom arrangement in a polycrystalline layer may be used to simulate randomly oriented atoms in channeling experiments if no preferred orientation of the grains exists. Then the dechanneling yield from a perfect crystal behind the evaporated layer should be inversely proportional to the energy E of the analyzing particles as has been shown by Bøgh[12]). This means that the ratio of the backscattering yields from a disordered (amorphous) layer to the dechanneling yield caused by this layer is proportional to E. Thus, in disordered crystals a direct backscattering peak should be always obtainable if the analyzing energy is high enough[13]). This however implies that no other defects are present in the crystal with a dechanneling cross-section increasing with E.

The dechanneling yield used in our experiments to test the energy dependence has been defined as the difference of the dechanneling yields normalized to the random spectra from the implanted and not implanted crystals at the same depth; random energy loss values have been assumed for all depth determinations. The results from the evaporated V layer are shown in fig. 1. Here on the left side, random and aligned backscattering spectra are plotted for 2 MeV $^4He^+$ particles. The yield from the layer is considerably reduced in comparison with the single crystal substrate due to oxygen incorporation during evaporation. The dechanneling yields $\Delta\chi$ (measured at a depth indicated by an arrow in the figure) are plotted as a function of E^{-1} on the right side of the figure and the expected linear relationship is found for the polycrystalline layer.

3.2. Implanted vanadium crystals

Backscattering spectra of aligned vanadium crystals bombarded with 2.9×10^{16} Ne^+/cm^2 at 320 keV are shown in fig. 2. The implantation energy of 320 keV has been chosen to simulate irradiation experiments with superconducting layers where Ne^+ ions of 320 keV penetrated 2000 Å thick layers generating damage along their paths and coming to rest in the substrate. The energy of the analyzing particles has been chosen as a parameter in the figure. All spectra are normalized to

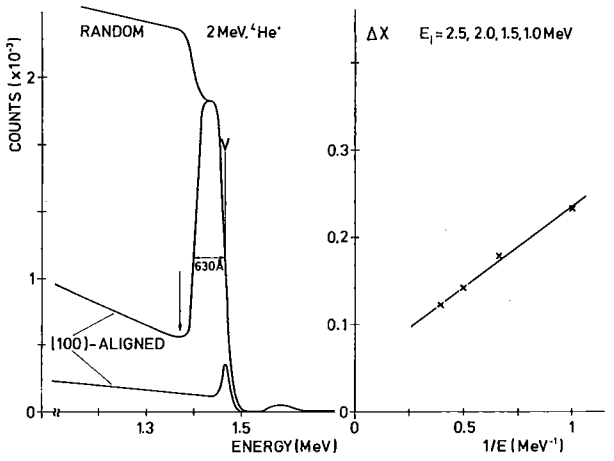

Fig. 1. Backscattering random and aligned spectra of a V layer evaporated onto a V single crystal. An aligned spectrum of a "pure" crystal is included for comparison (left). Dechanneling yield $\Delta\chi$ plotted as a function of the inverse analyzing beam energy (right).

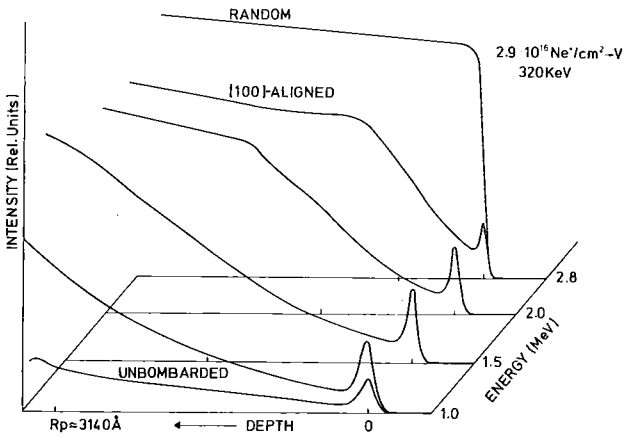

Fig. 2. Backscattering spectra of a [100] aligned V crystal bombarded with 2.9×10^{16} Ne^+/cm^2 320 keV, for different analyzing beam energies. A random (2.8 MeV) and an aligned (1.0 MeV) spectrum from an unbombarded crystal are included in the figure.

the same random height, to illustrate the change of the profiles, and a random (2.8 MeV) and an aligned spectrum (1.0 MeV) of unbombarded crystals are included in the figure for comparison. The depth scale is different for all energies and is indicated by the projected range of the Ne^+ ions. The dechanneling yield increases monotonically behind a surface disorder peak and extends to a characteristic "knee" well behind the ions projected range in accordance with earlier measurements[2,14]). However, no change of the shape of the spectra is observed with increasing $^4He^+$ particle energy.

In fig. 3 backscattering spectra from a nitrogen implanted (~10 at.%) vanadium crystal are shown in a plot similar to fig. 2. A dent in the random spectrum indicates the depth distribution of the implanted impurities. Here again a high dechanneling rate is observed; with increasing energy a well resolved disorder peak appears in the range of the implanted nitrogen atoms.

3.3. Implanted molybdenum crystals

In figs. 4 and 5 backscattering spectra from neon (10 at.%) and carbon (5 at.%) implanted molybdenum crystals are shown respectively. The same plotting procedure has been used as for the vanadium crystals. A high dechanneling yield increasing with depth and having a change in slope at the depth of the implanted atoms is observed for the neon implantation. In the carbon implanted sample, similar to nitrogen implanted into vanadium, a disorder peak appears in the spectra with increasing analyzing beam energy.

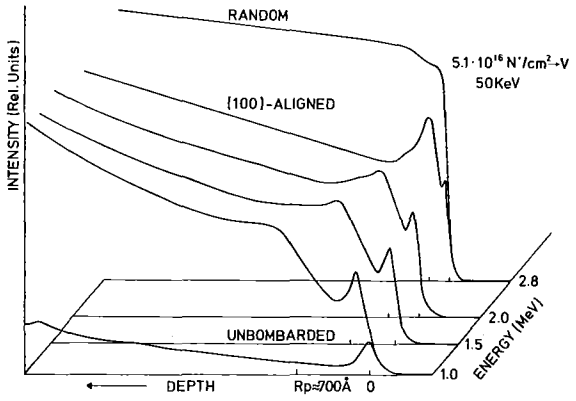

Fig. 3. Backscattering spectra of a [100] aligned V crystal implanted with 5.1×10^{16} N^+/cm^2 50 keV, at four different analyzing beam energies. Different depth scales in the spectra are indicated by the ions projected range R_p.

3.4. Dechanneling yields

The dechanneling yields $\Delta\chi$ from the implanted V and Mo crystals are plotted in figs. 6 and 7 as a function of E. The figures on the left show $\Delta\chi$ for the N or C implantations where disorder peaks appeared in the spectra and $\Delta\chi$ has been determined at a depth behind the disorder peak. The figures on the right show dechanneling yields at the three different depths indicated in each figure plotted for the Ne implantations. Straight line least-squares fits have been plotted through the points to indicate the energy dependence. For the N^+ and C^+ implantations in V and Mo a slight decrease of $\Delta\chi$ with increasing energy and high intersection values on the $\Delta\chi$ axis are observed. The Ne implanted samples reveal a different behaviour. Here an increase of the dechanneling yields

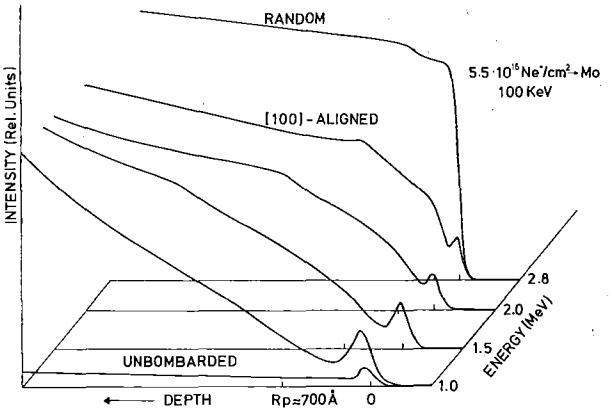

Fig. 4. Backscattering spectra of a [100] aligned Mo crystal bombarded with 5.5×10^{16} Ne^+/cm^2 100 keV. A dent in the random spectrum indicates the depth distribution of the Ne ions.

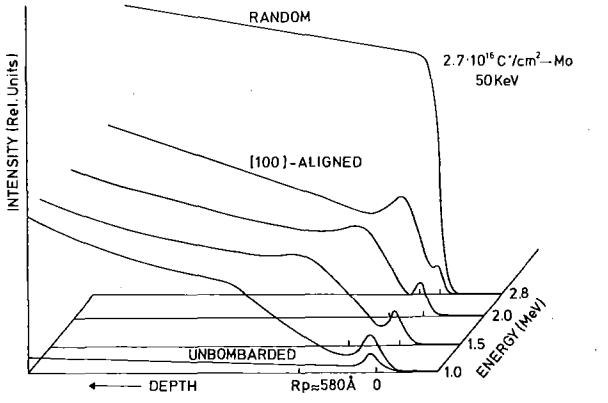

Fig. 5. Backscattering spectra of a [100] aligned Mo crystal implanted with 2.7×10^{16} C^+/cm^2 50 keV, with the analyzing beam energy as a parameter.

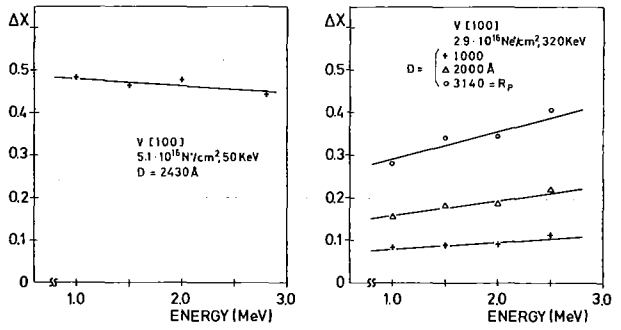

Fig. 6. Dechanneling yields $\Delta\chi$ from ion bombarded V crystals as a function of the analyzing beam energy. Left: $\Delta\chi$ at a depth $D = 2430$ Å (behind the disorder peak) for the N^+ implanted sample. Right: $\Delta\chi$ at three different depths for a Ne^+ implanted sample.

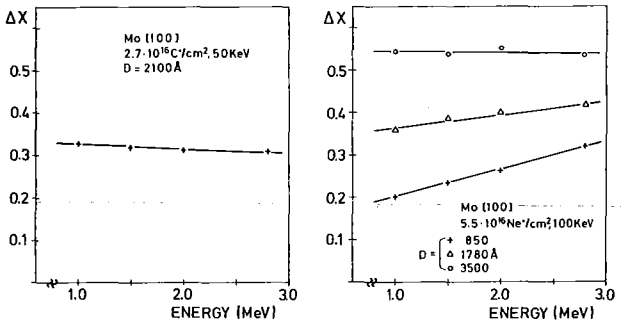

Fig. 7. Dechanneling yields $\Delta\chi$ from ion bombarded Mo crystals as a function of the analyzing beam energy. Left: $\Delta\chi$ at a depth $D = 2100$ Å (behind the disorder peak) for the C^+ implanted sample. Right: $\Delta\chi$ at three different depths for a Ne^+ bombarded sample.

vs energy is observed. The slope of this increase is most pronounced in the range of the implanted ions and decreases at depths beyond this range, then approaching an almost constant value. Plots of $\Delta\chi$ vs $\sqrt{E}$ for the Ne implantations also show high intersection values on the $\Delta\chi$ axis at depth beyond the ions range which are especially pronounced for Mo and less pronounced for V.

4. Discussion

The results described above show that for the Ne^+ ion implantations beyond the ions projected range a high amount of dechanneling is produced by defects causing an energy independent dechanneling yield. Thus from the energy dependence of the different types of defects present in metals it may be concluded that dechanneling is mainly due to stacking faults or voids. However within the Ne^+ ion range, plots vs $\sqrt{E}$ indicate the presence of dislocations or slightly misoriented regions though the interpretation is made complicated due to the scatter in the experimental points. In nitrogen or carbon implanted V and Mo crystals disorder peaks were observed at high analyzing energies but the dechanneling yield behind those peaks was much higher than would be caused by randomly displaced lattice atoms only. Thus here also the main portion of the dechanneling arises from defects having an energy independent dechanneling cross-section (concluded from the high intersection value on the $\Delta\chi$ axis). The slight decrease of $\Delta\chi$ with increasing energy here is due to that part of the disorder which gives rise to a direct backscattering peak. It is thought that these defects are lattice atoms displaced from the atomic rows, stabilized in their displaced positions by the implanted chemically active impurities (N^+, C^+). A random distribution of these defects in defect-impurity clusters is assumed from preliminary off axis dechanneling analysis as no change of the area of the disorder peak in slightly misaligned samples has been observed. A decrease of the dechanneling yield from such defects is in accordance with the E^{-1} energy dependence of randomly distributed atoms. This dependence however was difficult to verify quantitatively due to the small slope in the energy dependence, and the high energy independent dechanneling background.

5. Conclusion

The energy dependent dechanneling analysis on ion implanted V and Mo crystals has shown the presence of different types of defects in the bombarded samples, depending on the implanted impurities, implantation energy and depth. A high portion of defects has been found to cause energy independent dechanneling. A quantitative analysis separating the different types of defects however was difficult to perform because a small number of defects with a high dechanneling cross section may overshadow other defects which may be more concentrated but have a smaller dechanneling cross-section. In such cases, complementary analysis is necessary. Qualitatively however, different types of defects have been detected in Ne^+ or N^+ and C^+ implanted V and Mo crystals and the use of a high analyzing beam energy has proved favorable for the extraction of disorder peaks. Though the role of Ne in implantation experiments of su-

perconductors is yet not completely clear[11]) it is concluded that neon mainly gives rise to long range order defects like stacking faults or dislocations and that with N in V or C in Mo additional defects consisting of locally displaced lattice atoms are stabilized. Disorder introduced by these defects is thought to be the reason for the observed changes of the superconducting transition temperature in ion implanted V and Mo layers.

References

[1]) J. W. Mayer, L. Eriksson and J. A. Davies, *Ion implantation in semiconductors* (Academic Press, New York and London, 1970).

[2]) G. Linker, M. Gettings and O. Meyer, *Ion implantation in semiconductors and other materials* (ed. B. L. Crowder; Plenum Press, New York, 1973) p. 465.

[3]) P. P. Pronko, J. Bøttiger, J. A. Davies and J. B. Mitchell, Rad. Eff. **21** (1974) 25.

[4]) D. K. Sood and G. Dearnaley, J. Vac. Sci. Techn. **12** (1975) 445.

[5]) P. P. Pronko and K. L. Merkle, *Application of ion beams to metals* (eds. S. T. Picraux, E. P. EerNisse and F. L. Vook; Plenum Press, New York, 1974) p. 481.

[6]) Y. Quéré, Rad. Eff. **28** (1976) 253.

[7]) Y. Quéré, J. Nucl. Mat. **53** (1974) 262.

[8]) E. Rimini, S. U. Campisano, G. Foti, P. Baeri and S. T. Picraux, *Ion beam surface layer analysis* (eds. O. Meyer, G. Linker and F. Käppeler; Plenum Press, New York, 1976) p. 597.

[9]) O. Meyer, Inst. Phys. Conf. Ser. **28** (1976) 168.

[10]) G. Linker and O. Meyer, Sol. State Comm. **20** (1976) 695.

[11]) G. Linker, Int. Disc. Meet. on *Radiation effects in superconductivity,* Argonne (June 1977).

[12]) E. Bøgh, Can. J. Phys. **46** (1968) 653.

[13]) R. Behrisch and J. Roth, *Ion beam surface layer analysis* (eds. O. Meyer, G. Linker and F. Käppeler; Plenum Press, New York, 1976) p. 539.

[14]) M. Gettings, O. Meyer and G. Linker, Rad. Eff. **21** (1974) 51.

NUCLEAR INSTRUMENTS AND METHODS 149 (1978) 377-380 ; © NORTH-HOLLAND PUBLISHING CO.

CHANNELING EFFECT STUDIES IN V_3Si SINGLE CRYSTALS

O. MEYER

Kernforschungszentrum Karlsruhe, Institut für Angewandte Kernphysik, 7500 Karlsruhe, Postfach 3640, W. Germany

Angular scans through the [100] and [110] channeling directions in V_3Si have been performed using elastically scattered He ions for the V-rows and the $^{28}Si(d, p_8)^{29}Si$ reaction for the Si-rows. The amplitude of thermal vibration perpendicular to the V-chains was found to be larger than that at 45° to them. The Si atoms however vibrate isotropically. The use of multi-row potentials instead of single-row potentials leads to better overall agreement between measured and calculated critical angles.

1. Introduction

V_3Si is one of the well known superconducting compounds with A15-structure. In this class of material the superconducting transition temperature T_c is related to the linear chains of the transition metal atoms. The distance between adjacent V-atoms in the chains is smaller than the nearest next neighbour distance in bcc vanadium. From X-ray diffraction measurements[1]) it is known that the mean vibration amplitude perpendicular to the chain is larger than parallel to the row. Further, the phonon frequency distribution for the Si-atoms in V_3Si is found to be Einstein-like[2]) and a simple approach of using a Debye spectrum in calculating the mean vibrational amplitude is no longer valid. Both features offer interesting testing capabilities for the channeling technique.

2. Experimental

A V_3Si single crystal was cut almost perpendicular to the crystallographic [100] and [110] directions on opposite sides. Surfaces were lapped and polished with diamond paste and etched in a 1:1:1 mixture of H_2O:HF:H_2O_2.

Backscattering and channeling measurements were performed using a 3 MeV Van de Graaff accelerator. The sample was mounted on a three-axis-goniometer and a solid state detector was placed at 165° in order to determine the number and energy of the reaction products. Angular scan measurements for the V-rows were performed by elastically scattered He-ions from V-atoms, well separated in energy from those scattered from Si-atoms. χ_{min} is the minimum yield normalized to the random yield and $\psi_{1/2}$, the critical angle, is the half-angular width at half height between the minimum yield and the random yield. Two energy windows were used corresponding to two depth values near the surface and the results obtained for $\psi_{1/2}$ and χ_{min} were extrapolated to the target surface. The $^{28}Si(d, p_8)^{29}Si$ reaction was used for angular yield measurements from the Si-rows. Due to the low energy loss, the depth resolution is rather limited as confirmed by measuring the peak width for the proton yield from Si thin films of various thicknesses.

3. Analysis

Sectional areas through the atomic chains and the arrangement of the atoms in the chains parallel to the [100] and [110] channeling directions are shown in fig. 1. In the [110] direction there are Si- and V-rows with equal atomic distances, for the [100] direction the arrangement is more complicated as there are V-rows with different atomic distances d (strong rows V_s with $d=\frac{1}{2}a$ and weak rows V_w with $d=a$). Angular yield curves were taken in [100] as well as in [110] channeling directions.

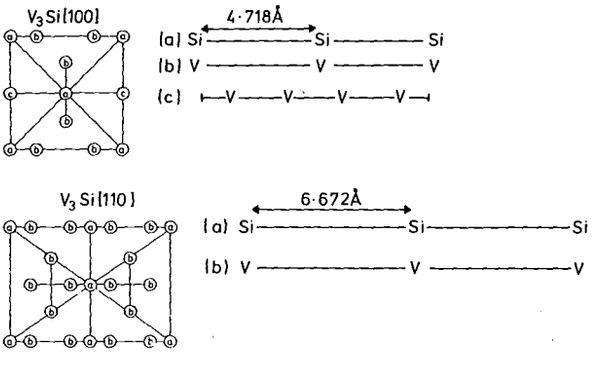

Fig. 1. Section areas through the atomic chains in V_3Si perpendicular to a ⟨100⟩ and a ⟨110⟩ plane and arrangement of atoms in different chains.

The measured $\psi_{1/2}$-values have been compared to values calculated with an empirical formula derived from Monte Carlo computer calculations[4]):

$$\psi_{1/2} = 0.8[V(1.2u_1)/E]^{\frac{1}{2}}, \quad (1)$$

with $V(r) = E\psi_1^2 f(r/a)$ where $V(r)$ is the continuum potential for a static row[4]) with Molière's screening function $f(r/a)\psi_1$ is the Lindhard characteristic angle[5]), u_1 is the average thermal vibrational amplitude perpendicular to the row, $1.2\,u_1$ is the distance of closest approach of channeled particles to the rows and at the Thomas–Fermi screening parameter ($a = 0.4685\,Z_2^{-\frac{1}{3}}$).

In complicated crystal structures such as V_3Si, rows with high scattering potentials (e.g. V-rows having small distances between the atoms) may affect the scattering potential of neighbouring weak rows. This influence can be estimated by following a procedure described in ref. 6. Potential-energy contour diagrams in planes perpendicular to the [100] and [110] directions have been determined using the continuum potential with Molière's screening function and considering the potential contribution from a matrix with a total of 79 atoms for the ⟨100⟩ and of 157 atoms for the ⟨110⟩ plane. From this calculation the multi-row potential $\Sigma V(1.2\,u_1)$ and V_0, the minimum potential in the open channels between the rows have been determined and the $\psi_{1/2}$-values have been calculated by inserting $\Sigma V(1.2\,u_1) - V_0$ in eq. (1).

The u_1-values for the V_3Si single crystals used in these experiments have been obtained from Debey temperatures of 394 K for the V- and of 628 K for the Si-sublattice as evaluated from neutron scattering experiments[2]). From these θ_b-values and assuming the Debye function for the phonon density distribution, the mean square of the displacement for an atom from the lattice position is usually calculated[7]).

The frequency distribution for Si in V_3Si is better reproduced by an Einstein function[2]): In such a case the following equation should be used[8]):

$$\langle u^2\rangle = 37.62\,T/(A\theta_2^2)\,[1 + \theta_{-2}^2/(36\,T^2) - \\ - \theta_{-2}^2\theta_2^2/(3600\,T^4) + \ldots], \quad (2)$$

which is valid for $T \geq 0.25\,\theta_b$. In eq. (2) θ_{-2} and θ_2 are the negative and positive second moments of the cut-off-temperature. In cases where θ_{-2} differs from θ_2 as for Si in V_3Si eq. (2) should be used.

The second parameter used for comparison between theory and experiment is the minimum yield. The analysis is based on an equation which was derived from Monte Carlo calculations[4]) for simple lattice structures: $\chi_{min} = 3\,\pi N d \times 2\,u_1^2$, where N is the density of target atoms and $\sqrt{3}\times\sqrt{2}\times u_1$ is interpreted as follows[6]): Particles incident parallel to the rows with impact parameters smaller than or equal to $\sqrt{3}\times\sqrt{2}\times u_1$ will be dechanneled and will then contribute to the minimum yield. For the case of complicated crystal structures the contributions from the different parallel rows have to be considered. For V_3Si, the more simple case is the [110] direction where parallel rows of either Si- or V-atom exist as can be seen from fig. 1.

The contribution of the Si-rows to $\chi_{min}^V[110]$ of the V-rows may be calculated by the procedure given in ref. 6:

$$\chi_{min}^V[110] = (18.6\,Ndu_1^2)_V + (\pi N d r_c^2)_{Si}. \quad (3)$$

r_c is determined from $V^{Si}(r_c) = V^V(\sqrt{6}\,u_1^V) - V_0$, where V^V is the potential of V-rows with the impact parameter $\sqrt{6}\times u_1^V$ as defined before. For the nuclear reaction part $\chi_{min}^{Si}[110]$ can be obtained in a similar way by just replacing V by Si and vice versa in eq. (3). For the [100] direction three types of rows V_s, V_w and Si exist as can be seen in fig. 1. $\chi_{min}^V[100]$ for the V part of the spectrum consists of contributions from V_s- and V_w-rows steering those particles into the other rows with deflection angles larger than $\psi_{1/2}$ of those rows:

$$\chi_{min}^V[100] = (18.8\,Ndu_1^2)_{V_s} + (18.8\,Ndu_1^2)_{V_w} + \\ + (\pi N d r_c^2)_{V_s} + (\pi N d r_c^2)_{V_w}. \quad (4)$$

Contributions from the Si-rows are small compared to the contributions given in eq. (4) and need not be considered. Minimum yield values for the reaction part are calculated by:

$$\chi_{min}^{Si}[100] = (18.8\,Ndu_1^2)_{Si} + (\pi N d r_c)_{V_s} + (\pi N d r_c^2)_{V_w}. \quad (5)$$

4. Results and discussion

As an example, angular scan curves for He ions through [100] and [110] crystal directions and elastically scattered from V-atoms together with the proton yield from the $^{28}Si(d, p_8)^{29}Si$ reaction are shown in fig. 2. The critical angles obtained from these angular scan measurements are summarized in table 1 and compared to values calculated from eq. (1) (column 3) and from eq. (1) with the multi row potential inserted (column 4). With V_0[100

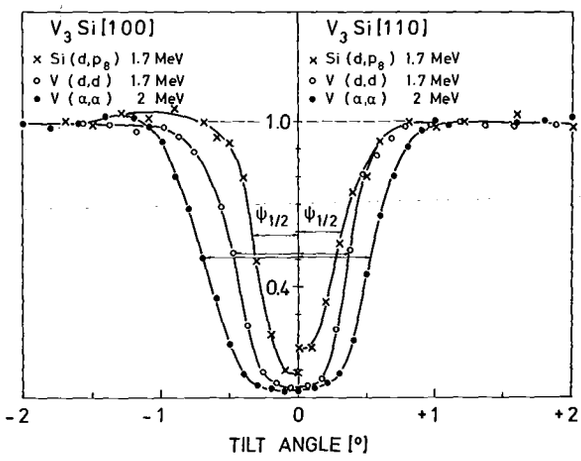

Fig. 2. Normalized yield as function of crystal orientation through the [100] and [110] directions. Elastic scattering of 2 MeV He ions and 1.7 MeV deuterons was used to measure $\psi_{1/2}$ and χ_{min} for the V-sublattice. The $^{28}Si(d, p_8)^{29}Si$ reaction was used to obtain $\psi_{1/2}$ and χ_{min} for the Si-rows separately.

being 37.7 eV and V_0[110] 27 eV, the $\psi_{1/2}$-values in the 4th column are smaller by about 0.03° and 0.02°, respectively. For deuterons in V_3Si the V_0 values are a factor of 2 smaller and no effect on $\psi_{1/2}$ is observed.

The $\psi_{1/2}$-values for the [100] direction are somewhat smaller than the theoretical values whereas the $\psi_{1/2}$-values for the [110] direction are found to be larger. The absolute $\psi_{1/2}$-value for the [110] has been confirmed by results from a second V_3Si single crystal using different tilt planes. Therefore it is concluded that the observed effect is due the anisotropic vibration of the V-atoms. The vibration amplitude perpendicular to the V-rows in the [100] direction is larger than the vibration amplitude at 45° to it in the [110] direction. This anisotropic vibration was not considered in the calculation. From eq. (1) with the multi-row potential the partial vibrational amplitudes are calculated by inserting the measured $\psi_{1/2}$-values to be $\langle u_{22}^2\rangle^V = 0.007$ Å^2 and $\langle u_{11}^2\rangle^V = 0.0025$ Å^2. From $\langle u^2\rangle^V = [\langle u_{11}^2\rangle + 2(\langle u_{22}^2\rangle^V)/3]$ a value of 0.0055 Å^2 is obtained in close agreement with the $\langle u_2^V\rangle$ value of 0.0053 Å^2, obtained from the isotropic Debye temperature for the V-sublattices evaluated from neutron experiments. The ratio of $\langle u_{11}^2\rangle/\langle u_{22}^2\rangle$ is equal to 0.36, a value that is small compared to the value of 0.8 found from X-ray analysis[1]).

The calculated $\psi_{1/2}$-values for the Si-rows are about 0.04° larger than the experimental values. As the measured values are not extrapolated to zero target thickness but are values averaged over a deep layer it is believed that the deviation from the calculated values is reasonable. As the experimental values in [100] and [110] channeling directions are smaller than the calculated $\psi_{1/2}$-values by the same amount, it is concluded that the Si atoms vibrate isotropically.

The second parameter used for comparison between theory and experiment is the minimum yield. In table 2 the measured values and those calculated from eqs. (3), (4) and (5) have been summarized. The mean vibration amplitudes used for the calculations have been obtained from eq. (1), inserting the experimental $\psi_{1/2}$-values and the multi-row potential for the V-sublattice. For the Si-sublattice the u_1-value as calculated from the Debye temperature has been used. The difference between the measured χ_{min}-values for the [100] and [110] Si-rows on one hand and the disagree-

TABLE 1

Experimental $\psi_{1/2}$-values and values $\psi_{1/2}^{calc}$, calculated for single-row and multi-row potentials.

Experiment	$\psi_{1/2}^{exp}$ (degrees)	$\psi_{1/2}^{calc}$ (Barrett) (degrees)	$\psi_{1/2}^{calc}$ multi-row pot. (Molière) (degrees)
V (α, α) [100] 2 MeV	0.75±0.02	0.81	0.78
V (α, α) [110] 2 MeV	0.52±0.02	0.49	0.47
Si (d, p_8) [100] 1.7 MeV	0.35	0.39	0.39
Si (d, p_8) [110] 1.7 MeV	0.29	0.33	0.34

TABLE 2

Experimental and calculated χ_{min}-values.

Experiment	χ_{min}^{exp}	χ_{min}^{calc}
V (α, α) [100] 2 MeV	0.018±0.003	0.034
V (α, α) [110] 2 MeV	0.020±0.003	0.020
Si (d, p_8) [100] 1.7 MeV	0.09	0.06
Si (d, p_8) [110] 1.7 MeV	0.18	0.05

ment between calculated and experimental values on the other hand is caused by experimental difficulties in the reaction analysis. For the elastically scattered He-ions the agreement between the experimental and theoretical χ_{min}-values is good for the [110] channeling direction where the contribution of the Si-rows to χ_{min} of the V-rows is only 10%. In the [100] channeling direction rather large contributions from the strong V-rows guiding He-particles into the weak rows and vice versa are calculated. The large discrepancy between measured and calculated χ_{min}-values for the [100] channeling direction indicate that theory has still to be modified. For the measured values for the [100] and [110] directions to be nearly equal is a further indication that the V-atom vibrates anisotropically.

The author wishes to thank R. Kaufmann for providing the program on multirow potential calculations and Dr. E. L. Haase for reading the manuscript.

References

[1] J. L. Staudenmann, P. Coppens and J. Müller, Sol. Stat. Comm. **19** (1976) 29.
[2] B.-P. Schweiß, B. Renker, E. Schneider and W. Reichardt, *Superconductivity in d- and f-band metals* (ed. D. H. Douglass; Plenum Press, N.Y., 1976).
[3] Single crystal V_3Si was obtained from B. Seeber, Universität München. Forschungslaboratorium für Festkörperchmie, Leiter: Dr. J. J. Nickl.
[4] J. H. Barrett, Phys. Rev. **B3** (1971) 1527.
[5] J. Lindhard, Kgl. Danske Videnskab. Selskab., Mat.-Fys. Medd. **34**, no. 14 (1965).
[6] D. S. Gemmell, and R. L. Mikkelsen, Phys. Rev. **B6** (1972) 1613.
[7] M. Blackman, *Handbuch der Physik,* vol. 7/1 (Springer Verlag, Berlin, 1955) p. 377.
[8] W. Reichardt, private communication.